DFG-Schwerpunktprogramm 1324

„Extraktion quantifizierbarer Information aus komplexen Systemen"

Effective discretization of direct reconstruction schemes for photoacoustic imaging in spherical geometries

F. Filbir, S. Kunis, R. Seyfried

Preprint 150

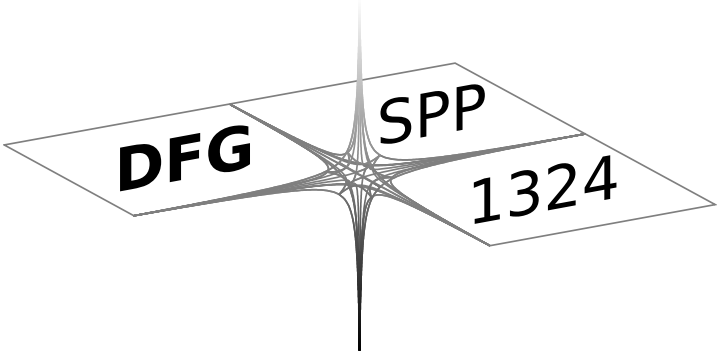

Edited by

AG Numerik/Optimierung
Fachbereich 12 - Mathematik und Informatik
Philipps-Universität Marburg
Hans-Meerwein-Str.
35032 Marburg

DFG-Schwerpunktprogramm 1324

„Extraktion quantifizierbarer Information aus komplexen Systemen”

Effective discretization of direct reconstruction schemes for photoacoustic imaging in spherical geometries

F. Filbir, S. Kunis, R. Seyfried

Preprint 150

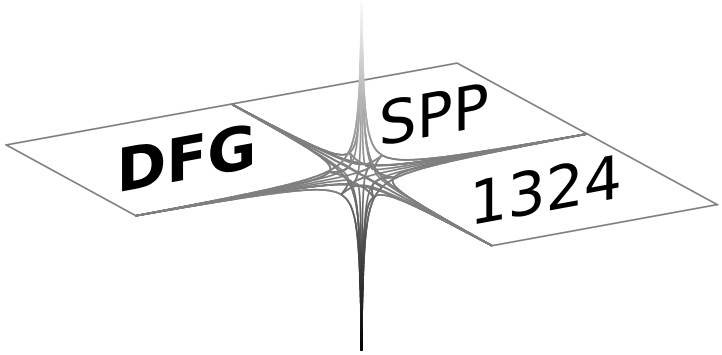

The consecutive numbering of the publications is determined by their chronological order.

The aim of this preprint series is to make new research rapidly available for scientific discussion. Therefore, the responsibility for the contents is solely due to the authors. The publications will be distributed by the authors.

Effective discretization of direct reconstruction schemes for photoacoustic imaging in spherical geometries

Frank Filbir [†] Stefan Kunis[‡] Ruben Seyfried[§]

Recently, kernel methods for the recovery of a function from its spherical means in spherical acquisition geometry have been proposed. We present efficient algorithms for these formulas in the two- and three-dimensional case. Our scheme applies Fourier techniques for certain convolution type integrals and discretizes physical space on a polar and spherical grid, respectively.

Key words and phrases : Radon transform, spherical means, fast Fourier transform.

2010 AMS Mathematics Subject Classification : 44A12, 65R32, 65T50, 92C55.

1 Introduction

Analogously to the inversion of the Radon transform in computerized tomography, recovering a function from its mean values over a family of spheres is relevant in photoacoustic tomography. The spherical mean operator $\mathcal{R} : C(\mathbb{R}^d) \to C(\mathbb{R}^d \times [0,\infty))$ is defined by

$$\mathcal{R}f(\xi,t) = \int_{\mathbb{S}^{d-1}} f(\xi + tu)\, \mathrm{d}\sigma(u),$$

where $\mathbb{S}^{d-1} = \big\{u \in \mathbb{R}^d : |u| = 1\big\}$ denotes the unit sphere and σ its surface measure with $\sigma(\mathbb{S}^1) = 2\pi$ and $\sigma(\mathbb{S}^2) = 4\pi$. The variable $t \geq 0$ is called measurement time and the variable $\xi \in \mathbb{R}^d$ detector position or center point. In all practical applications these center points are located on a curve or surface and we consider the classical case $\xi \in \mathbb{S}^{d-1}$ here. Moreover, we restrict ourselves to functions $f : \mathbb{R}^d \to \mathbb{R}$ with support $\mathrm{supp} f \subset \mathbb{B}$, where $\mathbb{B} = \big\{x \in \mathbb{R}^d : |x| < 1\big\}$ denotes the open unit ball, such that the spherical mean values $\mathcal{R}f(\xi,t)$ vanish for $t \geq 2$.

As outlined in [3, 1], the function f can be approximated from the spherical mean values $\mathcal{R}f(\xi,t)$, $\xi \in \mathbb{S}^{d-1}$, $t \in [0,2]$, using specific summability kernels. These kernels are families of

[§]Technische Universität München and Helmholtz Zentrum München, frank.filbir@helmholtz-muenchen.de
[‡]University Osnabrück and Helmholtz Zentrum München, stefan.kunis@math.uos.de
[§]Helmholtz Zentrum München, ruben.seyfried@helmholtz-muenchen.de

integrable functions $K_\varepsilon : \mathbb{B} \times \mathbb{B} \to \mathbb{R}$, where $\varepsilon \in (0,1)$ is a regularization parameter, with the properties

$$K_\varepsilon(x,y) = \int_{\mathbb{S}^{d-1}} k_\varepsilon(x,\xi,|y-\xi|)\ \mathrm{d}\sigma(\xi),$$
$$f(x) = \lim_{\varepsilon\to 0} \int_{\mathbb{B}} f(y) K_\varepsilon(x,y)\ \mathrm{d}y,$$

and $k_\varepsilon : \mathbb{B} \times \mathbb{S}^{d-1} \times [0,2] \to \mathbb{R}$ denotes some auxiliary function. Then a simple calculation shows, see [1, eq. (3)],

$$f(x) = \lim_{\varepsilon\to 0} \int_0^2 \int_{\mathbb{S}^{d-1}} k_\varepsilon(x,\xi,t) \mathcal{R}f(\xi,t)\ \mathrm{d}\sigma(\xi)\, t^{d-1}\ \mathrm{d}t.$$

Our main objective now is an effective discretization of this reconstruction formula for space dimensions $d = 2$ and $d = 3$. Towards this goal, we integrate over the sphere first and understand this step as a convolution for which Fourier techniques are applicable. This is followed by the integration over time and finally, an interpolation step on the reconstruction is performed.

Similar approaches can be found in [7, 6, 10] and references therein. The papers [7, 6] consider approximate reconstruction formulas in $d = 3$ and $d = 2$, respectively. The developed algorithm has three major steps: a filtering step that integrates the data $\mathcal{R}f(\xi,t)$ over time t against a kernel that depends only on the radial coordinate of the reconstruction position, a linear interpolation step on the intermediate data, and a subsequent backprojection step integrating over the sphere. Besides technicalities, this algorithm is efficient since the interpolation step basically decouples radial and angular coordinates. In contrast, our algorithm discretizes physical space on a polar or spherical grid, computes the inner integral of the reconstruction formula efficiently, and interpolates only the final result.

The algorithms in [10] implement exact reconstruction formulas by spectral methods which separate the radial and angular variables. After careful discretization and truncation of involved series, these schemes achieve optimal arithmetic complexity. The algorithms have four major steps: Fourier transforms with respect to time and also with respect to the angular component, a multiplication step, inverse Fourier transforms with respect to the angular component, an interpolation step from the polar or spherical grid to a Cartesian grid, and a final Fourier transform on the Cartesian grid. In contrast, we implement an *approximate* reconstruction formula and discretize on a polar or spherical in the original domain rather than in the frequency domain. Unfortunately, we do not achieve the optimal orders in arithmetic complexity, but as pointed out above our algorithms avoids interpolation of intermediate data.

The paper is organized as follows: We consider the two- and the three-dimensional case in Sections 2 and 3, respectively. After introducing the necessary notation, we first present the continuous version of the reconstruction formulas when considered in polar or spherical coordinates. Subsequently, we discretize these formulas on a polar or spherical grid, choose involved parameters and analyze the arithmetic complexity of the obtained algorithms. All theoretical results are illustrated by a couple of numerical experiments in Section 4 and we finally conclude our findings in Section 5.

2 Circular means

For the two-dimensional case $d = 2$, we consider detector positions on the unit circle , i.e. $\xi \in \mathbb{S}^1$, surrounding the support of the function f. For each detector position and measurement time $t \in [0, 2]$, the spherical mean is just the integral of f over a circular arc with midpoint ξ and radius t, see also Figure 2.1(left). An appropriate choice of the function k_ε now is

$$\begin{aligned} h : \mathbb{R} \to \mathbb{R}, \qquad & h(t) = \frac{1}{2\pi} \frac{1 - t^2}{(1 + t^2)^2}, \\ h_\varepsilon : [-2, 2] \to \mathbb{R}, \qquad & h_\varepsilon(t) = \frac{1}{\varepsilon^2} h(\frac{t}{\varepsilon}), \\ k_\varepsilon : \mathbb{B} \times \mathbb{S}^1 \times [0, 2] \to \mathbb{R}, \qquad & k_\varepsilon(x, \xi, t) = \frac{2}{\pi}(1 - |x|^2) h_\varepsilon(|x - \xi|^2 - t^2). \end{aligned}$$

The result that this indeed produces a summability kernel is given in [1, Corollary 2, Section (3.2)]. As a consequence we get an approximation to the function f by

$$f_\varepsilon(x) = \frac{2}{\pi}(1 - |x|^2) \int_0^2 \int_{\mathbb{S}^1} h_\varepsilon(|x - \xi|^2 - t^2) \mathcal{R}f(\xi, t) \, \mathrm{d}\sigma(\xi) \, t \, \mathrm{d}t. \tag{2.1}$$

Subsequently, we show that this reconstruction can be understood as a convolution when we use polar coordinates for the function f. Discretization leads to a polar grid as depicted in Figure 2.1(middle) and a bilinear interpolation on each polar wedge, cf. Figure 2.1(right) finally gives the reconstruction of f on a Cartesian grid.

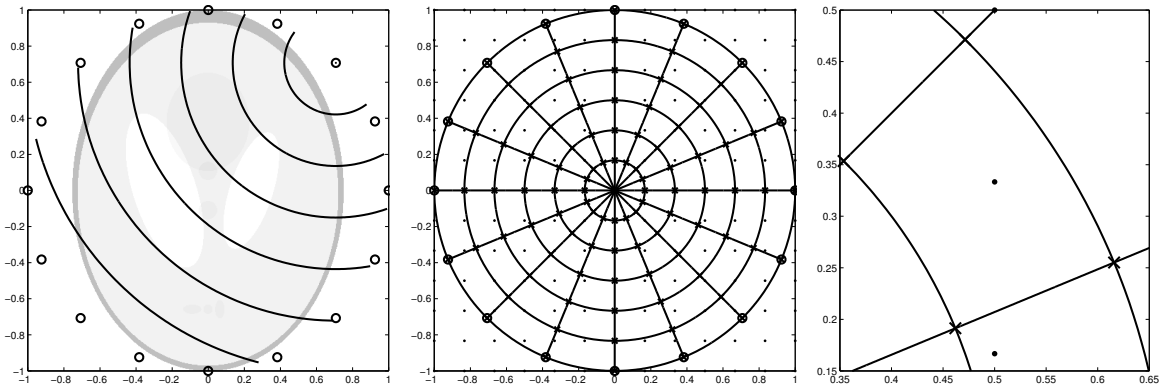

Figure 2.1: Measurement and reconstruction geometry.

Using the standard parameterization $\xi = (\cos\psi, \sin\psi)^\top$, $\psi \in [0, 2\pi)$, of the circle $\mathbb{S}^1$ and expressing $x \in \mathbb{B}$ in polar coordinates $x = r(\cos\varphi, \sin\varphi)^\top$, $r \in [0, 1)$, $\varphi \in [0, 2\pi)$, yields

$$|x - \xi|^2 = 1 + r^2 - 2r\cos(\psi - \varphi).$$

For notational convenience, we denote fixed arguments of functions as superscript and skipping the parameter ε completely, i.e.,

$$h^{r,t}(\psi) = h_\varepsilon(1 + r^2 - 2r\cos\psi - t^2),$$

$$g^t(\psi) = t \cdot \mathcal{R}f\left(\cos\psi, \sin\psi, t\right),$$

Hence, the approximation (2.1) can be written as a periodic convolution with respect to the angular component

$$f^{r,t}(\varphi) = \left(h^{r,t} * g^t\right)(\varphi) = \int_0^{2\pi} h^{r,t}(\varphi - \psi) g^t(\psi)\, \mathrm{d}\psi,$$
$$f_\varepsilon\left(r\cos\varphi, r\sin\varphi\right) = \frac{2}{\pi}(1-r^2)\int_0^2 f^{r,t}(\varphi)\, \mathrm{d}t.$$

Typically, the measurement times $t \in [0,2]$ are equidistant and the detector positions are equiangular $\xi_n = (\cos\psi_n, \sin\psi_n)^\top \in \mathbb{S}^1$,

$$t_m = \frac{2m}{M}, \qquad m = 0, \dots, M-1,$$
$$\psi_n = \frac{2\pi n}{N}, \qquad n = 0, \dots, N-1.$$

Thus, the integrals in (2.1) are discretized via composite quadrature rules with equidistant nodes. In the angular variable, constant weights give the highest trigonometric degree of exactness, in the time variable, constant weights yield a midpoint rule. We discretize the spatial variable $x \in \mathbb{B}$ accordingly on a polar grid $x_{\ell,j} = r_j(\sin\varphi_\ell, \cos\varphi_\ell)^\top$,

$$r_j = \frac{j}{J}, \qquad j = 0, \dots, J-1,$$
$$\varphi_\ell = \frac{2\pi\ell}{N}, \qquad \ell = 0, \dots, N-1,$$

which leads for fixed $\varepsilon \in (0,1)$ to the discrete reconstruction formula

$$f_\varepsilon(x_{\ell,j}) \approx f_\ell^j := \frac{8(1-|x_{\ell,j}|^2)}{MN} \sum_{m=0}^{M-1} f_\ell^{j,m} \tag{2.2}$$
$$f_\ell^{j,m} := \sum_{n=0}^{N-1} h_\varepsilon(1 + r_j^2 - t_m^2 - 2r_j\cos\psi_{n-\ell})\, t_m \cdot \mathcal{R}f(\xi_n, t_m)$$

For fixed indices j, m, the second sum is a multiplication with a circulant matrix, i.e., $\boldsymbol{f}^{j,m} = \boldsymbol{H}^{j,m}\boldsymbol{g}^m$, where

$$\boldsymbol{f}^{j,m} := (f_\ell^{j,m})_{\ell=0,\dots,N-1} \in \mathbb{R}^N,$$
$$\boldsymbol{g}^m := (t_m \cdot \mathcal{R}f(\xi_n, t_m))_{n=0,\dots,N-1} \in \mathbb{R}^N,$$
$$\boldsymbol{H}^{j,m} := (h_\varepsilon(1 + r_j^2 - t_m^2 - 2r_j\cos\psi_{n-\ell}))_{\ell,n=0,\dots,N-1} \in \mathbb{R}^{N\times N}.$$

We diagonalize $\boldsymbol{H}^{j,m} = \frac{1}{N}\boldsymbol{F}^* \operatorname{diag}\hat{\boldsymbol{h}}^{j,m}\boldsymbol{F}$ by a discrete Fourier transform, where

$$\boldsymbol{F} := (\mathrm{e}^{-2\pi\mathrm{i}kn/N})_{k,n=0,\dots,N-1},$$
$$\hat{\boldsymbol{h}}^{j,m} := \boldsymbol{F}\boldsymbol{h}^{j,m},$$
$$\boldsymbol{h}^{j,m} := (h_\varepsilon(1 + r_j^2 - t_m^2 - 2r_j\cos\psi_n))_{n=0,\dots,N-1}.$$

We bring the inverse Fourier transform in front of the outer summation in (2.2) and have the following Algorithm 1.

Algorithm 1

Input : discretization parameter $N, M, J \in \mathbb{N}$,
measurement times $t_m = \frac{2m}{M}$, $m = 0, \dots, M-1$,
detector positions $\xi_n = (\cos\psi_n, \sin\psi_n)$, $\psi_n = \frac{2\pi n}{N}$, $n = 0, \dots, N-1$,
data $\mathcal{R}f(\xi_n, t_m)$, $n = 0, \dots, N-1$, $m = 0, \dots, M-1$,
radii $r_j = \frac{j}{J}$, $j = 0, \dots, J-1$,
angles $\varphi_\ell = \frac{2\pi\ell}{N}$, $\ell = 0, \dots, N-1$.

Output : function values $f_l^j \approx f_\varepsilon(r_j \cos\varphi_\ell, r_j \sin\varphi_\ell)$, $\ell = 0, \dots, N-1$, $j = 0, \dots, J$

for $j = 0, \dots, J-1$ ***do***
  for $m = 0, \dots, M-1$ ***do***
    set $\boldsymbol{g}^m = (t_m \cdot \mathcal{R}f(\xi_n, t_m))_{n=0,\dots,N-1}$
    compute $\hat{\boldsymbol{f}}^{j,m} = \operatorname{diag}(\hat{\boldsymbol{h}}^{j,m})\boldsymbol{F}\boldsymbol{g}^m$
  end for
  compute $\hat{\boldsymbol{f}}^j = \frac{8(1-r_j^2)}{MN^2} \sum_{m=0}^{M-1} \hat{\boldsymbol{f}}^{j,m}$
  compute $\boldsymbol{f}^j = \boldsymbol{F}^* \hat{\boldsymbol{f}}^j$
end for

Remark 2.1. *Finally, the function f needs to be evaluated on a Cartesian grid and since the reconstruction yields function values on the polar grid, we employ the following interpolation scheme, see also Figure 2.1(middle). Let the discretization parameter $L \in \mathbb{N}$ and nodes $z_{s,t} = (s/L, t/L)$, $s,t = -L, \dots, L$, be given. For ease of notation, consider some fixed node $z_{s,t}$ in the positive quadrant with $\|z_{s,t}\|_2 < 1$, define indices and weights*

$$j = \left\lfloor \frac{J\sqrt{s^2+t^2}}{L} \right\rfloor, \qquad w_{s,t,j} = J\left(\frac{\sqrt{s^2+t^2}}{L} - r_j\right),$$
$$\ell = \left\lfloor \frac{N}{2\pi} \arctan\frac{t}{s} \right\rfloor, \qquad v_{s,t,\ell} = \frac{N}{2\pi}\left(\arctan\frac{t}{s} - \varphi_\ell\right),$$

and interpolate bilinearly in the polar grid by

$$\begin{aligned}\tilde{f}_\varepsilon(z_{s,t}) = (1-w_{s,t,j})\,(1-v_{s,t,\ell})\,f_l^j + w_{s,t,j}\,(1-v_{s,t,\ell})\,f_l^{j+1} \\ + (1-w_{s,t,j})\,v_{s,t,\ell} f_{l+1}^j + w_{s,t,j} v_{s,t,\ell} f_{l+1}^{j+1}.\end{aligned} \tag{2.3}$$

Figure 2.1(right) illustrates part of the polar grid and one evaluation node $z_{s,t}$ in its polar wedge. Alternatively, one might use a nearest neighbor interpolation in the polar grid or a constant or linear interpolation over some triangulation of the polar grid.

2.1 Parameter choice and computational complexity

An important question concerns the choice of the parameter ε, see also [6, Section 5.1]. While the approximation (2.1) becomes better for smaller ε, the discretization of the outer integral by a composite midpoint rule produces reasonable results only if the integrand is smooth with respect to the mesh size M^{-1} in (2.2). Since the function h_ε has its main lobe in the interval $[-\varepsilon, \varepsilon]$ and a constant number $C \geq 1$ of samples should lie inside this interval, we set

$$\varepsilon = \frac{C}{M},$$

which can further decreased by an artificial increase of the resolution of the measurements, e.g., by interpolation.

The inner sum in (2.2) is a discrete and cyclic convolution and can be realized by means of fast Fourier transforms in $\mathcal{O}(N \log N)$ floating point operations. Taking into account the outer summation over time in (2.2) for all radii, this leads to $\mathcal{O}(JMN \log N)$ floating point operations. Interpolation of the result in (2.3) is a local operation and takes only $\mathcal{O}(JN + L^2)$ floating point operations. Assuming finally $\mathcal{O}(J) = \mathcal{O}(L) = \mathcal{O}(M) = \mathcal{O}(N)$ and considering the total problem size $n = N^2$, our algorithm has complexity $\mathcal{O}(n^{1.5} \log n)$. We note in passing, that the polar grid discretization might be coarsened near the origin saving a fraction of the total computations and that a generalization to nonequally spaced detectors on the unit circle is straightforward using the nonequispaced FFT [9].

3 Spherical means

For the three-dimensional case $d = 3$, we consider detector positions on the unit sphere, i.e. $\xi \in \mathbb{S}^2$, surrounding the support of the function f, see Figure 3.1(left). For each detector position and measurement time $t \in [0, 2]$, the spherical mean is just the integral of f over a spherical cap with midpoint ξ and radius t, see also Figure 3.1(right).

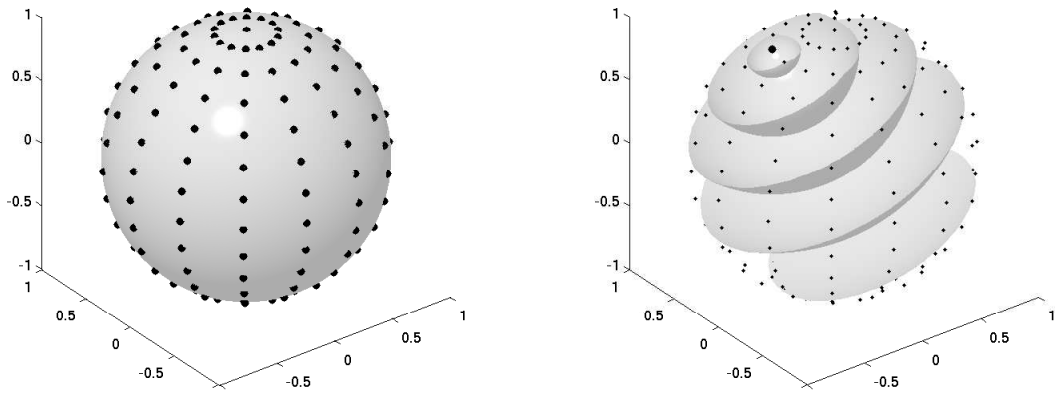

Figure 3.1: Measurement geometry.

Now the results in [1, Theorem 4, Section (4.2)] give rise to a whole family of reconstruction formulas. Let $q \in \mathbb{N}$, $q \geq 2$, be given and define $c_q = \frac{4\Gamma\left(q+\frac{5}{2}\right)}{\sqrt{\pi}\Gamma(q+1)}$. Let $(t)_+ = \max\{t, 0\}$,

$$\begin{aligned} h_q : \mathbb{R} \to \mathbb{R}, \qquad & h_q(t) = c_q \left[\left(1 - t^2\right)_+^q - 2qt^2 \left(1 - t^2\right)_+^{q-1} \right], \\ h_{\varepsilon,q} : [-2, 2] \to \mathbb{R}, \qquad & h_{\varepsilon,q}(t) = \frac{1}{\varepsilon^3} h_q(\frac{t}{\varepsilon}), \\ k_{\varepsilon,q} : \mathbb{B} \times \mathbb{S}^2 \times [0, 2] \to \mathbb{R}, \qquad & k_{\varepsilon,q}(x, \xi, t) = \frac{(1 - |x|^2)}{2\pi^2} h_{\varepsilon,q}(|x - \xi|^2 - t^2). \end{aligned} \tag{3.1}$$

The conditions of [1, Theorem 4] are satisfied since the function h_q is even, locally integrable,

$h_q(t) = c_q \frac{\mathrm{d}}{\mathrm{d}t} t(1-t^2)_+^q$, and the function $H_q : \mathbb{R}^3 \to \mathbb{R}$,

$$H_q(x) := \frac{1}{4\pi} \int_{\mathbb{S}^2} h_q(\langle x, \xi \rangle) \, \mathrm{d}\sigma(\xi) = \frac{1}{|x|} \int_{-|x|}^{|x|} h_q(t) \, \mathrm{d}t = \frac{c_q}{4\pi} (1 - |x|^2)_+^q,$$

is a radial, $\int_{\mathbb{R}^3} H_q(x) \, \mathrm{d}x = 1$, and $|H_q(x)| \leq 16(1 + |x|)^{-4}$. Hence, the function f can be approximately reconstructed by

$$f_\varepsilon(x) = \frac{(1 - |x|^2)}{2\pi^2} \int_0^2 \int_{\mathbb{S}^2} h_{\varepsilon,q}(|x - \xi|^2 - t^2) \mathcal{R}f(\xi, t) \, \mathrm{d}\sigma(\xi) \, t^2 \, \mathrm{d}t. \tag{3.2}$$

Subsequently, we propose a reconstruction scheme generalizing the convolution type ideas. We express the spatial variable in spherical coordinates, cf. Figure 3.2(left), generalize the convolution on the circle $\mathbb{S}^1$ to the sphere $\mathbb{S}^2$, and diagonalize the convolutions by means of appropriate fast spherical Fourier transform. Two other approaches, one based on a discretization in cylinder coordinates, cf. Figure 3.2(right), and another one using the compact support of the function $h_{\varepsilon,q}$, are discussed in Section 3.2.

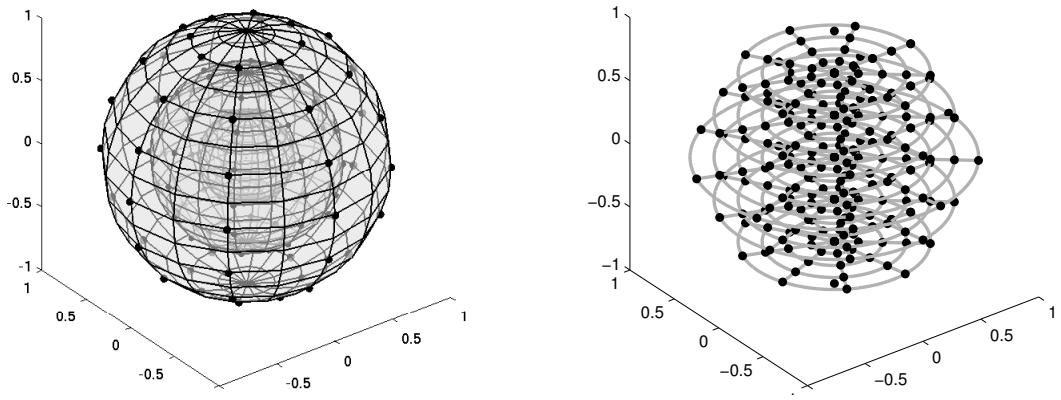

Figure 3.2: Reconstruction geometries, spherical (left) and cylindrical coordinates (right).

Expressing $x \in \mathbb{B}$ in spherical coordinates $x = r\eta$, $r \in [0, 1)$, $\eta \in \mathbb{S}^2$, cf. Figure 3.2(left), yields

$$|x - \xi|^2 = 1 + r^2 - 2r\eta \cdot \xi.$$

We write fixed arguments of functions as superscript and suppress the parameters ε and q completely, i.e.,

$$\begin{aligned} h^{r,t} : [-1, 1] \to \mathbb{R}, \qquad & h^{r,t}(y) = h_{\varepsilon,q}(1 + r^2 - t^2 - 2ry), \\ g^t : \mathbb{S}^2 \to \mathbb{R}, \qquad & g^t(\xi) = t^2 \mathcal{R}f(\xi, t), \end{aligned} \tag{3.3}$$

the approximation (3.2) can be written as a convolution of a function on the sphere with a zonal kernel and a subsequent integration

$$f^{r,t}(\eta) = \left(h^{r,t} * g^t\right)(\eta) = \int_{\mathbb{S}^2} h^{r,t}(\eta \cdot \xi) g^t(\xi) \, \mathrm{d}\sigma(\xi), \tag{3.4}$$

$$f_\varepsilon(x) = f_\varepsilon(r\eta) = \frac{(1-r^2)}{2\pi^2} \int_0^2 f^{r,t}(\eta)\,\mathrm{d}t.$$

In order to get a fast algorithm for the convolution (3.4), we follow [8] and expand the function $h^{r,t}$ in a Legendre series. The Legendre-Polynomials $P_k : [-1,1] \to \mathbb{R}$ are defined as

$$P_k(x) = \frac{1}{2^k k!} \frac{\mathrm{d}}{\mathrm{d}x} \left(x^2-1\right)^k,$$

by $Y_k^n : \mathbb{S}^2 \to \mathbb{C}$ we denote the spherical harmonic of degree $k \in \mathbb{N}_0$ and order $n = -k, \dots, k$. We use the addition theorem for spherical harmonics, which separates the dependencies of the variables η and ξ in

$$h^{r,t}(\eta \cdot \xi) = \sum_{k=0}^{\infty} \hat{h}_k^{r,t} P_k(\eta \cdot \xi) = \sum_{k=0}^{\infty} \frac{4\pi \hat{h}_k^{r,t}}{2k+1} \sum_{n=-k}^{k} Y_k^n(\eta)\overline{Y_k^n(\xi)}, \tag{3.5}$$

where the Fourier Legendre coefficients are given by

$$\hat{h}_k^{r,t} = \frac{2k+1}{2} \int_{-1}^{1} h^{r,t}(x) P_k(x)\,\mathrm{d}x. \tag{3.6}$$

Since the sum in (3.5) converge absolutely, which follows from Theorem 3.4, we can interchange the order of summation and integration, this yields

$$f_\varepsilon(r\eta) = \frac{2}{\pi}(1-r^2) \sum_{k=0}^{\infty} \sum_{n=-k}^{k} Y_k^n(\eta) \int_0^2 \frac{\hat{h}_k^{r,t}}{2k+1} \int_{\mathbb{S}^2} g^t(\xi)\overline{Y_k^n(\xi)}\,\mathrm{d}\sigma(\xi)\,\mathrm{d}t. \tag{3.7}$$

Both integrals are discretized at the locations where the data $\mathcal{R}f(\xi,t)$ is given, i.e., the inner integral at the detector positions and the outer integral at the measurement times

$$\begin{aligned} \xi_i &\in \mathbb{S}^2, & i &= 0, \dots, I^2-1, \\ t_m &= \frac{2m}{M}, & m &= 0, \dots, M-1. \end{aligned}$$

We evaluate the function f_ε at points $x_{j,l} = r_j \eta_l$, where

$$\begin{aligned} \eta_l &\in \mathbb{S}^2, & l &= 0, \dots, L^2-1, \\ r_j &= \frac{j}{J}, & j &= 0, \dots, J-1. \end{aligned}$$

Moreover, we approximate the series expansion of h^{r_j,t_m} as given in (3.5) at a fixed cut-off degree $N \in \mathbb{N}$ and compute the Fourier coefficients in this series by a quadrature,

$$\hat{h}_k^{r_j,t_m} \approx \hat{h}_k^{j,m} := \sum_{\nu=0}^{N-1} \mu_\nu P_k(\lambda_\nu) h^{r_j,t_m}(\lambda_\nu).$$

Provided $N > 2q$ and the Gauß Legendre nodes and weights (λ_ν, μ_ν) are chosen for the support of $h^{r,t}$, this quadrature is exact since $h^{r,t}$ is a polynomial of degree $2q$ within its support. The resulting truncation error is discussed in Section 3.1.

Our algorithm now works as follows. In a first step and for each measurement time t_m individually, we compute discrete spherical Fourier coefficients

$$\hat{g}^m_{n,k} := \sum_{i=0}^{I^2-1} \omega_i \overline{Y^n_k(\xi_i)} g^{t_m}(\xi_i), \quad k = 0, \dots, N-1,\ n = -k, \dots, k,$$

approximating the inner integral in (3.7) by numerical quadrature on the nodes $\xi_i \in \mathbb{S}^2$ and with some weights $\omega_i > 0$, $i = 0, \dots, I^2 - 1$. These computations are realized via an adjoint nonequispaced fast spherical Fourier transform (adjoint NFSFT), see e.g. [9], the accuracy of this approximation and a precomputation of the weights is discussed in [5].

In a second step and for each radius r_j individually, we compute

$$\hat{f}^j_{n,k} := \frac{2}{M} \sum_{m=0}^{M-1} \frac{\hat{h}^{j,m}_k}{2k+1} \hat{g}^m_{n,k}, \quad k = 0, \dots, N-1,\ n = -k, \dots, k, \tag{3.8}$$

approximating the outer integral in (3.7) by numerical quadrature at the nodes t_m and with constant weights $\frac{2}{M}$. Finally, we evaluate the truncated outer sum in (3.7) at the target nodes η_l, $l = 0, \dots, L^2 - 1$, i.e.,

$$f_\varepsilon(r_j \eta_l) \approx f^j_l := \frac{2(1-r_j^2)}{\pi} \sum_{k=0}^{N} \sum_{n=-k}^{k} \hat{f}^j_{n,k} Y^n_k(\eta_l), \quad l = 0, \dots, L^2 - 1, \tag{3.9}$$

by a nonequispaced fast spherical Fourier transform (NFSFT). For notational convenience, we define

$$\begin{aligned}
\boldsymbol{g}^m &:= \big(\omega_i g^{t_m}(\xi_i)\big)_{i=0,\dots,I^2-1} = \big(\omega_i t_m^2 \mathcal{R} f(\xi_i, t_m)\big)_{i=0,\dots,I^2-1} \in \mathbb{R}^{I^2} \\
\boldsymbol{Y}_\xi &:= \big(Y^n_k(\xi_i)\big)_{i=0,\dots,I^2-1;\ k=0,\dots,N-1,\ n=-k,\dots,k} \in \mathbb{C}^{I^2 \times N^2}, \\
\boldsymbol{Y}_\eta &:= \big(Y^n_k(\eta_l)\big)_{l=0,\dots,L^2-1;\ k=0,\dots,N-1,\ n=-k,\dots,k} \in \mathbb{C}^{L^2 \times N^2}.
\end{aligned}$$

and formulate Algorithm 2.

Remark 3.1. *The reconstruction yields function values on the spherical grid, see also Figure 3.2(left). Analogously to Remark 2.1, we interpolate trilinear in the spherical grid. We assume $\eta \in \mathbb{S}^2$ is given in the form*

$$\eta_{\ell,n} = \left(\sin(\psi_\ell)\cos(\varphi_n), \sin(\psi_\ell)\sin(\varphi_n), \cos(\psi_\ell)\right)^\top, \qquad \varphi_\ell = \frac{2\pi\ell}{L},\ \psi_n = \frac{\pi n}{L-1},$$

$\ell = 0, \dots, L-1$, $n = 0, \dots, L-1$, and Algorithm 2 outputs values $f^j_{\ell,n} \approx f_\varepsilon(r_j \eta_{\ell,n})$. Let the discretization parameter $K \in \mathbb{N}$ and Cartesian nodes $z_{s,t,w} = \left(\frac{s}{K}, \frac{t}{K}, \frac{p}{K}\right)$, $s,t,p = -K, \dots, K$, be given. For ease of notation, consider some fixed node $z_{s,t,p}$ with $\|z_{s,t,p}\|_2 < 1$ and define the corresponding indices and weights by

$$\begin{aligned}
j &= \left\lfloor \frac{J\sqrt{s^2+t^2+p^2}}{K} \right\rfloor, & w_j &= J\left(\frac{\sqrt{s^2+t^2+p^2}}{K} - r_j\right), \\
\ell &= \left\lfloor \frac{L}{2\pi}\left(\pi + \operatorname{sgn}(t) \arccos \frac{s}{\sqrt{s^2+t^2}}\right)\right\rfloor, & v_\ell &= \frac{L}{2\pi}\left(\pi + \operatorname{sgn}(t) \arccos \frac{s}{\sqrt{s^2+t^2}} - \varphi_\ell\right),
\end{aligned}$$

$$n = \left\lfloor \frac{L-1}{\pi} \left(\arccos \frac{p}{\sqrt{s^2+t^2+p^2}} \right) \right\rfloor, \qquad u_n = \frac{L-1}{\pi} \left(\arccos \frac{p}{\sqrt{s^2+t^2+p^2}} - \psi_n \right).$$

Now, interpolate along φ, ψ, and r respectively, by

$$\begin{aligned}
c_{00} &= (1-v_\ell) f^j_{\ell,n} + v_\ell f^j_{\ell+1,n}, & c_{01} &= (1-v_\ell) f^j_{\ell,n+1} + v_\ell f^j_{\ell+1,n+1},\\
c_{10} &= (1-v_\ell) f^{j+1}_{\ell,n} + v_\ell f^{j+1}_{\ell+1,n}, & c_{11} &= (1-v_\ell) f^{j+1}_{\ell,n+1} + v_\ell f^{j+1}_{\ell+1,n+1},\\
c_0 &= (1-u_n) c_{00} + u_n c_{01}, & c_1 &= (1-u_n) c_{10} + u_n c_{11},\\
\tilde{f}_\varepsilon(z_{s,t,p}) &= (1-w_j) c_0 + w_j c_1.
\end{aligned}$$

Algorithm 2

Input : discretization parameter $I, M, L, J, N \in \mathbb{N}$,
measurement times $t_m = \frac{2m}{M}$, $m = 0, \dots, M-1$,
detector positions $\xi_i \in \mathbb{S}^2$, $i = 0, \dots, I^2-1$,
data $\mathcal{R}f(\xi_i, t_m)$, $i = 0, \dots, I^2-1$, $m = 0, \dots, M-1$
radii $r_j = \frac{j}{J}$, $j = 0, \dots, J-1$,
angles $\eta_l \in \mathbb{S}^2$, $l = 0, \dots, L^2-1$.

Output : function values $f^j_l \approx f_\varepsilon(r_j \eta_l)$, $l = 0, \dots, L^2-1$, $j = 0, \dots, J-1$.

for $m = 0, \dots, M-1$ ***do***
  set $\boldsymbol{g}^m = \big(\omega_i t_m^2 \mathcal{R}f(\xi_i, t_m)\big)_{i=0,\dots,I^2-1}$
  compute $\hat{\boldsymbol{g}}^m = \boldsymbol{Y}^*_\xi \boldsymbol{g}^m$
end for
for $j = 0, \dots, J-1$ ***do***
  for $k = 0, \dots, N-1$ ***do***
    for $m = 0, \dots, M-1$ ***do***
      compute $\hat{h}^{j,m}_k = \sum_{\nu=0}^{N-1} \mu_\nu P_k(\lambda_\nu) h^{r_j, t_m}(\lambda_\nu)$
    end for
    for $n = -k, \dots, k$ ***do***
      compute $\hat{f}^j_{n,k} = \frac{4(1-r_j^2)}{(2k+1)M\pi} \sum_{m=0}^{M-1} \hat{h}^{j,m}_k \hat{g}^m_{n,k}$
    end for
  end for
  compute $\boldsymbol{f}^j = \boldsymbol{Y}_\eta \hat{\boldsymbol{f}}^j$
end for

3.1 Parameter choice and computational complexity

It remains to choose the parameters $q, N \in \mathbb{N}$, $\varepsilon > 0$, and analyze the final computational complexity of Algorithm 2. Similar to Section 2.1, we subsequently argue that the regularization parameter ε is bounded with respect to the discretization of the measurement time, i.e., $\varepsilon \geq CM^{-1}$. Moreover, the parameter $q \in \mathbb{N}$ determines the smoothness of the function $h^{r,t}$ and thus the asymptotic decay of its Fourier Legendre coefficients (3.6). Theorem 3.4 makes this observation precise and allows for an error estimate in Corollary 3.5 which also shows that the asymptotic decay sets in for $k \geq C\varepsilon^{-1}$. Hence, the choice $N = CM$ of the cut-off degree allows for a guaranteed accuracy and a complexity estimate of Algorithm 2.

For notational convenience, we drop all parameters from the considered function $h : \mathbb{R} \to \mathbb{R}$,

$$h(y) := h^{r,t}(y) = h_{\varepsilon,q}(1 + r^2 - t^2 - 2ry).$$

Since

$$\text{supp } h = [v - u, v + u], \quad v := \frac{1 + r^2 - t^2}{2r},\ u := \frac{\varepsilon}{2r}, \tag{3.10}$$

we obtain that supp $h \cap [-1, 1] \neq \emptyset$ if and only if

$$t \in \left[\sqrt{((1-r)^2 - \varepsilon)_+}, \sqrt{(1+r)^2 + \varepsilon}\right].$$

Consequently, we have $\hat{h}_k \neq 0$ and thus nonzero terms in the sum (3.8) only if $m = M_1, \ldots, M_2$, where

$$M_1 = \left\lceil \frac{M}{2}\sqrt{((1-r_j)^2 - \varepsilon)_+} \right\rceil, \quad M_2 = \min\left\{ \left\lfloor \frac{M}{2}\sqrt{(1+r_j)^2 + \varepsilon} \right\rfloor, M - 1 \right\}$$

and this speeds up the total computations. On the other hand, the sum (3.8) represents the integration over t and is a reasonable discretization only if at least a constant number of samples are taken into account. Considering the critical case $r = 0$, dropping the rounding, and using

$$M_2 - M_1 \geq \frac{M}{2}\left(\sqrt{1+\varepsilon} - \sqrt{1-\varepsilon}\right) \geq \frac{M\varepsilon}{2},$$

this is the case for $\varepsilon = C/M$.

We proceed by estimating the Fourier Legendre coefficients (3.6). Trivially, all coefficients fulfill $\hat{h}_k = 0$, $k \in \mathbb{N}_0$, if supp $h \cap [-1, 1] = \emptyset$, and we have $\hat{h}_k = 0$, $k \geq 2q+1$, if $[-1, 1] \subset$ supp h. Subsequently, we discuss the remaining case and set

$$[a, b] := \text{supp } h \cap [-1, 1]. \tag{3.11}$$

We start by bounding the coefficients $\hat{h}_k$ independently of k in Lemma 3.2 and compute the values of the function h and its derivatives in the endpoints of its support in Lemma 3.3. This allows for the estimate on the decay of the Fourier Legendre coefficients $\hat{h}_k$ in Theorem 3.4.

Lemma 3.2. *The Fourier-Legendre coefficients* (3.6) *fulfill*

$$\left|\hat{h}_k\right| \leq \frac{4q(q+1)c_q}{\varepsilon^3},$$

where c_q *is given in* (3.1).

Proof. First note, that $h'(a) = h'(b) = 0$ if $-1 < a < b < 1$ and that $P_k(1) = 1$ and $P_k(-1) = (-1)^k$, $k \in \mathbb{N}_0$. In combination with

$$(2k+1)P_k = P'_{k+1} - P'_{k-1}, \quad k \in \mathbb{N}, \tag{3.12}$$

integration by parts leads to

$$\left|\hat{h}_k\right| = \frac{2k+1}{2}\left|\int_a^b h(s)P_k(s)\,\mathrm{d}s\right| \leq \frac{1}{2}\int_a^b \left|h'(s)\right| \left|P_{k+1}(s) - P_{k-1}(s)\right|\,\mathrm{d}s.$$

Using $|P_k(s)| \le 1$ and

$$|h'(s)| = \frac{2qc_q|(v-s)|}{\varepsilon^3 u^{2q}}(u^2-(v-s)^2)_+^{q-2}\left|3u^2-(2q+1)(v-s)^2\right| \le \frac{4q(q+1)c_q}{\varepsilon^3 u} \le \frac{8q(q+1)c_q}{\varepsilon^3(b-a)}$$

which follows from $\max_{s\in[a,b]}|v-s| \le \max_{s\in[v-u,v+u]}|v-s| = u$, $(u^2-(v-s)^2)_+ \le u^2$, and $2u \ge b-a$, the assertion follows. ∎

Lemma 3.3. *The function h and its derivatives of order $p = 0,\dots,2q$ fulfill*

$$h^{(p)}(v+u) = \begin{cases} 0 & \text{if } p = 0,\dots,q-2, \\ \frac{(-1)^q 2^{2q-1-p}(p+2)!c_q}{\varepsilon^3 u^p (q+1)}\binom{q+1}{p-q+1} & \text{if } p = q-1,\dots,2q, \end{cases}$$

and $h^{(p)}(v-u) = (-1)^p h^{(p)}(v+u)$, see (3.1) for the definition of c_q.

Proof. We consider the auxiliary function $g_q(s) = (u^2-(v-s)^2)^q = (u-v+s)^q(u+v-s)^q$ which fulfills

$$\begin{aligned} g_q^{(p)}(s) &= \sum_{i=0}^{p}\binom{p}{i}\frac{\mathrm{d}^{p-i}}{\mathrm{d}s^{p-i}}(u-v+s)^q\frac{\mathrm{d}^i}{\mathrm{d}s^i}(u+v-s)^q \\ &= \begin{cases} \sum_{i=0}^{p}\binom{q}{i}\binom{q}{p-i}(-1)^i p!(u-v+s)^{q-p+i}(u+v-s)^{q-i} & \text{if } p<q, \\ \sum_{i=(p-q)}^{q}\binom{q}{i}\binom{q}{p-i}(-1)^i p!(u-v+s)^{q-p+i}(u+v-s)^{q-i} & \text{if } p\ge q, \end{cases} \end{aligned}$$

and as a consequence

$$g_q^{(p)}(v+u) = \begin{cases} 0 & \text{if } p<q, \\ (-1)^q\binom{q}{p-q}p!(2u)^{2q-p} & \text{if } p\ge q. \end{cases}$$

The assertion follows from $g_q^{(p)}(v-u) = (-1)^p g_q^{(p)}(v+u)$ and

$$h(s) = \frac{(2q+1)c_q}{\varepsilon^3}u^{-2q}g_q(s) - \frac{2qc_q}{\varepsilon^3}u^{-2(q-1)}g_{q-1}(s).$$

∎

Theorem 3.4. *The Fourier Legendre coefficients $\hat{h}_k$ of the function h obey the inequality*

$$\left|\hat{h}_k\right| \le \frac{C_q\sqrt{u}\left((1-b^2)^{\frac{1}{4}}+(1-a^2)^{\frac{1}{4}}\right)}{\varepsilon^3\sigma^{q-\frac{1}{2}}}\left(2+\frac{1}{\sigma}\right)^{q+1}, \quad k > 2q+1,$$

where $a<b$ are given by (3.11), $\sigma = u(k-2q)$, $C_q = (2q+1)!c_q$, and c_q is given in (3.1).

Proof. For notational convenience let $[f]_a^b := f(b)-f(a)$. Induction over $p = 1,\dots,2q$, using integration by parts together with equation (3.12), yields

$$\begin{aligned} |\hat{h}_k| \le{}& \frac{1}{2}\sum_{i=0}^{p-1}\frac{1}{2^i(k-(p-1))^i}\sum_{l=0}^{i}\binom{i}{l}\left|\left[h^{(i)}(P_{k-i+2l+1}-P_{k-i+2l-1})\right]_a^b\right| \\ &+\frac{1}{2}\frac{1}{2^{p-1}(k-(p-1))^{p-1}}\sum_{l=0}^{p}\binom{p}{l}\left|\int_a^b h^{(p)}(s)P_{k-p+2l}(s)\,\mathrm{d}s\right| \end{aligned}$$

$$\leq \frac{1}{2}\sum_{i=0}^{2q}\frac{1}{(2(k-2q))^i}\sum_{l=0}^{i}\binom{i}{l}\left|\left[h^{(i)}(P_{k-i+2l+1}-P_{k-i+2l-1})\right]_a^b\right|, \tag{3.13}$$

where the last step for $p=2q$ is due to $h_q^{(2q)}$ being constant. We use the inequality

$$|P_{k+1}(x)-P_{k-1}(x)| \leq \frac{2(1-x^2)^{\frac{1}{4}}}{\sqrt{k}}, \quad k\geq 2,\ x\in[-1,1],$$

see [2] and [11, p. 172, eq. (7.33.10)] for a related asymptotic statement. Since $[a,b]\subsetneq[-1,1]$, we assume that $b<1$.Together with the symmetry of the derivatives, this provides

$$\begin{aligned}\left|\left[h^{(i)}(P_{k-i+2l+1}-P_{k-i+2l-1})\right]_a^b\right| &\leq \left|h^{(i)}(b)\right|\frac{2(1-b^2)^{\frac{1}{4}}}{\sqrt{k-i+2l}}+\left|h^{(i)}(a)\right|\frac{2(1-a^2)^{\frac{1}{4}}}{\sqrt{k-i+2l}}\\ &\leq \frac{2\left|h^{(i)}(b)\right|}{\sqrt{k-i}}\left((1-b^2)^{\frac{1}{4}}+(1-a^2)^{\frac{1}{4}}\right),\end{aligned}$$

where the corresponding term on the right hand side vanishes if $a=-1$. We proceed in (3.13) by

$$\begin{aligned}\left|\hat{h}_k\right| &\leq \sum_{i=0}^{2q}\frac{(1-b^2)^{\frac{1}{4}}+(1-a^2)^{\frac{1}{4}}}{(2(k-2q))^i}\frac{\left|h^{(i)}(b)\right|}{\sqrt{k-i}}\sum_{l=0}^{i}\binom{i}{l}\\ &= \left((1-b^2)^{\frac{1}{4}}+(1-a^2)^{\frac{1}{4}}\right)\sum_{i=0}^{2q}\frac{1}{(k-2q)^i}\frac{\left|h^{(i)}(b)\right|}{\sqrt{k-i}}.\end{aligned}$$

Applying Lemma 3.3, we get

$$\begin{aligned}\sum_{i=0}^{2q}\frac{1}{(k-2q)^i}\frac{\left|h^{(i)}(b)\right|}{\sqrt{k-i}} &\leq \frac{c_q}{\varepsilon^3}\sum_{i=q-1}^{2q}\frac{2^{2q-1-i}}{(k-2q)^{i+\frac{1}{2}}u^i}\binom{q+1}{i-q+1}\frac{(i+2)!}{q+1}\\ &\leq \frac{c_q(2q+1)!}{\varepsilon^3}\sum_{i=q-1}^{2q}\frac{2^{2q-i}}{(k-2q)^{i+\frac{1}{2}}u^i}\binom{q+1}{i-q+1}\\ &= \frac{c_q(2q+1)!\sqrt{u}}{\varepsilon^3\sigma^{q-\frac{1}{2}}}\sum_{i=0}^{q+1}\frac{2^{q+1-i}}{\sigma^i}\binom{q+1}{i}\end{aligned}$$

and the assertion follows by the binomial theorem. ∎

Corollary 3.5. *Let $\varepsilon\in(0,1)$, $N\in\mathbb{N}$, $N\geq 2/\varepsilon$, and the approximation f_ε in (3.2) be truncated by $f_\varepsilon^N:\mathbb{B}\to\mathbb{R}$,*

$$f_\varepsilon^N(r\eta)=\frac{(1-r^2)}{2\pi^2}\int_0^2\int_{\mathbb{S}^2}h^N(\eta\xi)g^t(\xi)\,\mathrm{d}\sigma(\xi)t^2\,\mathrm{d}t, \quad h^N=\sum_{k=0}^{N+2q-1}\hat{h}_kP_k,$$

where $r\in(0,1)$ and $\eta\in\mathbb{S}^2$, then

$$\|f_\varepsilon-f_\varepsilon^N\|_\infty\leq\frac{\tilde{C}_q(1-r^2)r^{q-1}}{\varepsilon^{\frac{7}{2}}}(\varepsilon N)^{\frac{3}{2}-q}\|f\|_\infty,$$

where $\tilde{C}_q=32\cdot 6^{q+1}\cdot C_q$.

Proof. Using $\max_{x\in[-1,1]} |P_k(x)| = 1$, we get

$$\begin{aligned}
|f_\varepsilon(r\eta) - f_\varepsilon^N(r\eta)| &\le \frac{1-r^2}{2\pi^2} \int_0^2 \int_{\mathbb{S}^2} \left|h(\eta\xi) - h^N(\eta\xi)\right| \left|g^t(\xi)\right| |t|^2 \,\mathrm{d}\sigma(\xi)\,\mathrm{d}t \\
&\le \frac{1-r^2}{2\pi^2} \sum_{k=N+2q}^{\infty} |\hat{h}_k| \int_0^2 \int_{\mathbb{S}^2} \int_{\mathbb{S}^2} |f(\xi+tu)| \,|t|^2 \,\mathrm{d}\sigma(u)\,\mathrm{d}\sigma(\xi)\,\mathrm{d}t \\
&\le \frac{2^6(1-r^2)}{3} \|f\|_\infty \sum_{k=N+2q}^{\infty} |\hat{h}_k|.
\end{aligned}$$

Applying Theorem 3.4 together with $2 + \frac{1}{\sigma} \le 3$ and $u = \frac{\varepsilon}{2r}$, the sum of the Fourier Legendre coefficients is bounded by

$$\sum_{k=N+2q}^{\infty} |\hat{h}_k| \le \frac{2\ 3^{q+1} C_q}{\varepsilon^3 u^{q-1}} \sum_{k=N}^{\infty} k^{\frac{1}{2}-q} \le \frac{2\ 3^{q+1} C_q}{\varepsilon^3 u^{q-1}} \left(N^{\frac{1}{2}-q} + \int_N^\infty x^{\frac{1}{2}-q}\,\mathrm{d}x \right) \le \frac{2\ 3^{q+2} C_q (2r)^{q-1}}{\varepsilon^{\frac{7}{2}} (\varepsilon N)^{q-\frac{3}{2}}}.$$

■

The constants in the above estimate are not optimized in any way and numerical experiments suggest that the actual error includes an additional factor $N^{-\frac{1}{2}}$. In total, the truncation error decays algebraically with a rate depending on the smoothness parameter q and this behavior sets in for $N \ge \varepsilon^{-1}$.

Remark 3.6. *Regarding the total accuracy of Algorithm 2, we note the following.*

i) Approximating the function f by (3.2) induces the approximation error

$$\|f - f_\varepsilon\|_\infty,$$

whose discussion, in particular its so called degree of approximation with respect to ε and q, is beyond the scope of this paper.

ii) Corollary 3.5 discusses the truncation error

$$\|f_\varepsilon - f_\varepsilon^N\|_\infty$$

and suggests a choice of the truncation parameter N with respect to ε.

iii) Finally, the discrete spherical Fourier coefficients $\hat{g}_{k,n}^m$ of the given data are computed by a quadrature rule. Together with the discretization of the integral over the measurement time, this introduces a discretization error

$$\max_{j,l} |f_\varepsilon^N(r_j\eta_l) - f_j^l|.$$

Provided the detector positions are somewhat uniformly distributed on the sphere, we expect a degree of exactness $N \approx I$ and a rate of convergence $N^{-q'}$ where q' is related to the smoothness of the given data, see also [5]. The integral over the measurement time is computed by a simple trapezoidal rule whose accuracy is discussed e.g. in [12].

The above discussion supports the parameter choice $\varepsilon = \mathcal{O}(1/M)$, $N = \mathcal{O}(M)$, and moreover, we assume $\mathcal{O}(I) = \mathcal{O}(J) = \mathcal{O}(N)$. Each spherical Fourier transforms in Algorithm 2 is computed in $\mathcal{O}(N^2 \log^2 N)$ floating point operations and thus, the most time consuming parts rely on the two innermost loops. Hence, we have a total complexity of $\mathcal{O}(n^{\frac{4}{3}})$ floating point operations with respect to the total problem size $n = N^3$.

3.2 Compact support and cylindrical coordinates

Subsequently, we shortly discuss two other approaches to discretize the reconstruction formula (3.2). Using the compact support of the function $h_{\varepsilon,q}$ and after changing the order of integration, we obtain

$$f_\varepsilon(x) = \frac{(1-|x|^2)}{2\pi^2} \int_{\mathbb{S}^2} \int_{\sqrt{(|x-\xi|^2-\varepsilon)_+}}^{\min\{2,\sqrt{|x-\xi|^2+\varepsilon}\}} h_{\varepsilon,q}(|x-\xi|^2 - t^2) \mathcal{R}f(\xi,t)\, t^2 \,\mathrm{d}t \,\mathrm{d}\sigma(\xi).$$

For simplicity, we consider the case of a single discretization parameter $N \in \mathbb{N}$ and reconstruct f on the Cartesian grid $x_{\ell,p,j} = \frac{1}{N^3}(\ell,p,j)^\top \in [-1,1]^3$, $\ell,p,j = -N,\dots,N$. Discretizing the outer integral by N^2 nodes on $\mathbb{S}^2$ and the inner integral over the original interval $[0,2]$ by N nodes leads for fixed indices l,p,j to

$$f_\varepsilon(x_{l,p,j}) \approx \frac{2c_q(1-|x_{l,p,j}|^2)}{N^3} \sum_{i=1}^{N} \sum_{n=1}^{N} \sum_{m=N_1}^{N_2} h_{\varepsilon,q}(|x_{l,p,j}-\xi_{i,n}|^2 - t_m^2) \mathcal{R}f(\xi_{i,n},t_m)\, t_m^2 \sin\psi_{1,i}.$$

In case $|x_{l,p,j}-\xi_{i,n}|^2 \geq \varepsilon$, we have

$$\begin{aligned}
(N_2-N_1)^2 &\leq N^2 \left(\sqrt{|x_{l,p,j}-\xi_{i,n}|^2+\varepsilon} - \sqrt{|x_{l,p,j}-\xi_{i,n}|^2-\varepsilon} \right)^2 \\
&= 2N^2 \left(|x_{l,p,j}-\xi_{i,n}|^2 - \sqrt{|x_{l,p,j}-\xi_{i,n}|^4-\varepsilon^2} \right) \\
&\leq 2N^2 \left(|x_{l,p,j}-\xi_{i,n}|^2 - \sqrt{(|x_{l,p,j}-\xi_{i,n}|^2-\varepsilon)^2} \right) = 2\varepsilon N^2,
\end{aligned}$$

in case $|x_{l,p,j}-\xi_{i,n}|^2 < \varepsilon$ even simpler $N_2 - N_1 = N\sqrt{|x_{l,p,j}-\xi_{i,n}|^2+\varepsilon} \leq \sqrt{2\varepsilon}N$. Assuming as above $\varepsilon = CN^{-1}$, this yields $N_2 - N_1 = \mathcal{O}(\sqrt{N})$ and thus, with respect to the total problem size $n = N^3$, a total complexity of $\mathcal{O}(n^{\frac{11}{6}})$ floating point operations.

The second approach is a direct generalization of the two-dimensional case, where we express the spatial variable in cylinder coordinates and thus reconstructs f for each fixed third Cartesian coordinate separately, cf. Figure 3.2(right). We use the parameterization $\xi = (\sin\psi_1\cos\psi_2, \sin\psi_1\sin\psi_2, \cos\psi_1)^\top$, $\psi_1 \in [0,\pi]$, $\psi_2 \in [0,2\pi)$, of the sphere $\mathbb{S}^2$ and express $x \in \mathbb{B}$ in cylindrical coordinates $x = (r\cos\varphi, r\sin\varphi, z)^\top$, $r \in [0,1)$, $z \in (-1,1)$, $\varphi \in [0,2\pi)$, which yields

$$|x-\xi|^2 = 1 + r^2 + z^2 - 2r\sin\psi_1\cos(\psi_2-\varphi) - 2z\cos\psi_1.$$

Denoting fixed arguments of functions as superscript and skipping the parameters ε and q completely, i.e.,

$$\begin{aligned}
h^{r,t,z,\psi_1}(\psi_2) &= h_{\varepsilon,q}(1+r^2+z^2-2r\sin\psi_1\cos(\psi_2)-2z\cos\psi_1-t^2), \\
g^{t,\psi_1}(\psi_2) &= t^2 \cdot \mathcal{R}f(\sin\psi_1\cos\psi_2, \sin\psi_1\sin\psi_2, \cos\psi_1, t),
\end{aligned}$$

the approximation (3.2) can be written as a periodic convolution with respect to the angular component

$$f^{r,t,\psi_1,z}(\varphi) = \left(h^{r,t,\psi_1,z} * g^{\psi_1,t} \right)(\varphi) = \int_0^{2\pi} h^{r,t,\psi_1,z}(\varphi-\psi_2) g^{t,\psi_1}(\psi_2) \,\mathrm{d}\psi_2,$$

$$f_\varepsilon(r\cos\varphi, r\sin\varphi, z) = \frac{1}{2\pi^2}(1-r^2-z^2)\int_0^2\int_0^\pi f^{r,t,\psi_1,z}(\varphi)\sin\psi_1\,\mathrm{d}\psi_1\,\mathrm{d}t.$$

We assume, similar to the two-dimensional case, equidistant measurement times $t \in [0,2]$ and equiangular detector positions $\xi_{i,n} = (\sin\psi_{1,i}\cos\psi_{2,n}, \sin\psi_{1,i}\sin\psi_{2,n}, \cos\psi_{1,i})^\top \in \mathbb{S}^2$,

$$\begin{aligned} t_m &= \frac{2m}{M}, && m = 0,\dots,M-1,\\ \psi_{1,i} &= \frac{\pi i}{I-1}, && i = 0,\dots,I-1,\\ \psi_{2,n} &= \frac{2\pi n}{N}, && n = 0,\dots,N-1. \end{aligned}$$

Furthermore, we discretize the spatial variable $x \in \mathbb{B}$ in cylindrical coordinates $x_{\ell,p,j} = (r_j\sin\varphi_\ell, r_j\cos\varphi_\ell, z_p)^\top$,

$$\begin{aligned} z_p &= \frac{2p+1-P}{P}, && p = 0,\dots,P-1,\\ r_j &= \frac{j}{J}, && j = 0,\dots,J_p-1,\ J_p = \left\lfloor\sqrt{1-z_p^2}\cdot J\right\rfloor,\\ \varphi_\ell &= \frac{2\pi\ell}{N}, && \ell = 0,\dots,N-1, \end{aligned}$$

which leads to the discrete reconstruction formula

$$f_\varepsilon(x_{\ell,p,j}) \approx f_l^{j,p} := \frac{2(1-r_j^2-z_p^2)}{(I-1)MN}\sum_{m=0}^{M-1}\sum_{i=0}^{I-1}\sin\psi_{1,i} f_\ell^{j,m,p,i} \tag{3.14}$$

$$f_\ell^{j,m,p,i} := \sum_{n=0}^{N-1} h_{\varepsilon,q}(1+r_j^2+z_p^2-2z_p\cos\psi_{1,i}-t_m^2-2r_j\sin\psi_{1,i}\cos\psi_{2,n-l})t_m^2\mathcal{R}f(\xi_{i,n},t_m).$$

Using the idea of Algorithm 1 for each third spatial coordinate z_p individually, this approach is of particular interest if one needs to reconstruct f on a few horizontal planes only. For fixed j,m,p,i, the inner sum again is a discrete and cyclic convolution and realized by means of fast Fourier transforms in $\mathcal{O}(N\log N)$ floating point operations. Taking into account the outer summations over time and angle in (3.14) for all radii and angles, assuming that all discretization parameters are of order $\mathcal{O}(N)$, and considering the total problem size $n = N^3$ this leads to $\mathcal{O}(n^{5/3}\log n)$ floating point operations.

4 Numerical results

The implementation of Algorithm 1 and Algorithm 2 is realized in MATLAB and we use a Lenovo Thinkpad T60, 4GByte, Intel(R) Core(TM)2 Duo CPU P8700 2.53GHz for all numerical experiments. Besides introductory examples, our interest is the computation time for increasing discretization parameters and the accuracy with respect to the involved parameters.

4.1 Circular means

We start by some introductory example using the well known Shepp Logan phantom, see Figure 4.1(left). As for the ordinary Radon transform, its circular mean values can be computed

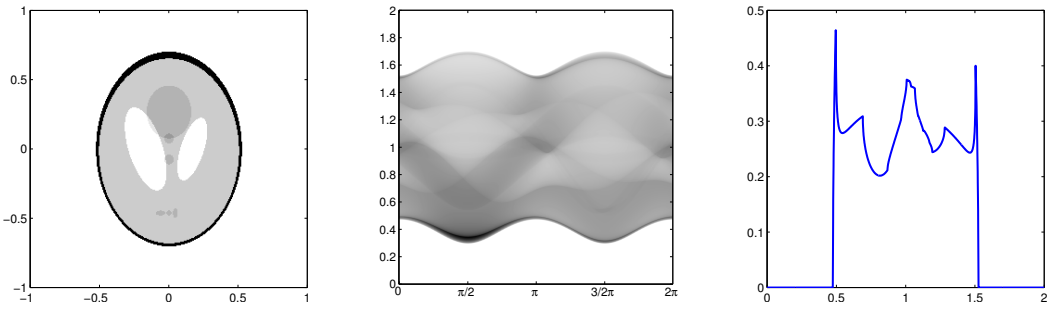

Figure 4.1: Shepp Logan phantom (left) and circular mean values (middle) together with a profile for $\xi = (0,1)^\top$ (right).

analytically [4], Figure 4.1(middle & right) show the entire data and a profile for $\xi = (0,1)^\top$, respectively.

The input of Algorithm 1 are these spherical means $\mathcal{R}f(\xi_n, t_m)$, $n = 0, \dots, N-1$, $m = 0, \dots, M-1$, for discretization parameters $N = 360$ and $M = 2000$. We reconstruct the phantom f on a polar grid with $J = 600$ radii and set the regularization parameter to $\varepsilon = 5 \cdot 10^{-3}$. Figure 4.2(left & middle) shows the reconstruction on a Cartesian grid and a profile for $x_{(2)} = 0$, clearly visible is a smoothing effect on the jump singularities leading also to a damping of small details.

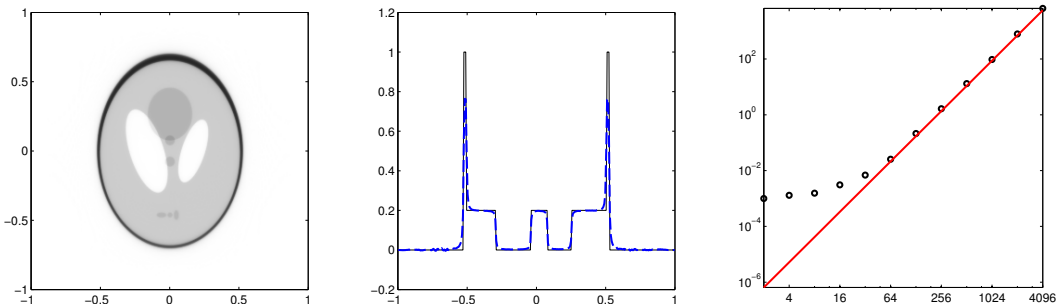

Figure 4.2: Reconstruction of the Shepp Logan phantom, on a Cartesian grid (left) and a profile for $x_{(2)} = 0$ (middle). Computation times in seconds with respect to the common discretization parameter (right).

For the discussion of accuracy and computation time, we consider the function $f : \mathbb{R}^2 \to \mathbb{R}$,

$$f(x) = \left(1 - \frac{|x-a|^2}{0.6^2}\right)_+^3, \quad a = \frac{1}{5}(1,1)^\top,$$

We fix the regularization parameter $\varepsilon = 10^{-2}$, choose discretization parameters $N = M = J = 2^l$, $l = 1, \dots, 12$, and interpolate to a Cartesian grid with $L = 2^{l-1}$ grid points in each coordinate, see Remark 2.1. Figure 4.2(right) shows the computation time for the reconstruction with interpolation together with the estimated order $\mathcal{O}\left(N^3\right)$, where we neglected the logarithmic term. The total accuracy of Algorithm 1 is measured by

$$E_\infty = \max_{\ell,j} |f(x_{\ell,j}) - f_l^j|, \tag{4.1}$$

and we consider this quantity for fixed parameters $N = J = 500$ and $M = 8000$ and a decreasing regularization parameter $\varepsilon = 2^{-l}$, $l = 1, \dots, 10$. Table 4.1 shows an error behavior $E_\infty \approx 2.8\varepsilon$ until the discretization becomes too coarse at $\varepsilon \approx \frac{8}{M}$ resulting in an increasing error.

ε	2^{-1}	2^{-2}	2^{-3}	2^{-4}	2^{-5}
E_∞	$7.1 \cdot 10^{-1}$	$4.9 \cdot 10^{-1}$	$3.0 \cdot 10^{-1}$	$1.6 \cdot 10^{-1}$	$8.6 \cdot 10^{-2}$
ε	2^{-6}	2^{-7}	2^{-8}	2^{-9}	2^{-10}
E_∞	$4.4 \cdot 10^{-2}$	$2.2 \cdot 10^{-2}$	$1.1 \cdot 10^{-2}$	$5.7 \cdot 10^{-3}$	$4.9 \cdot 10^{-2}$

Table 4.1: Error of the reconstruction with respect to the regularization parameter.

4.2 Spherical means

We start again by some simple test-function as depicted in Figure 4.3(left). The spherical means of this superposition of characteristic functions on balls are computed analytically [4]. Figure 4.3(middle & right) show a equatorial cross section for $\xi_{(3)} = 0$ and a profile for $\xi = (1, 0, 0)^\top$ of these mean values, respectively.

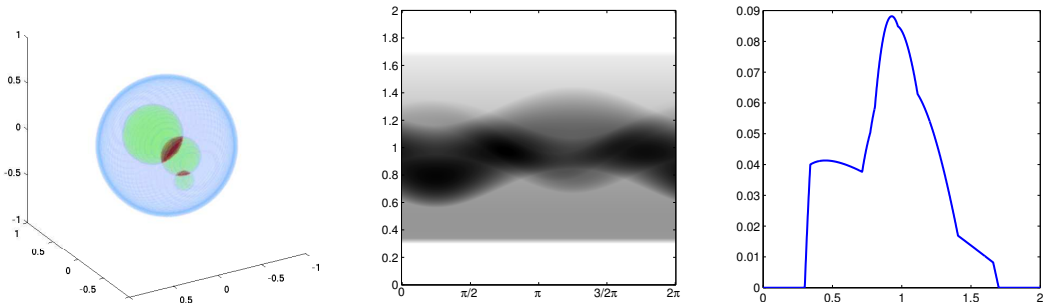

Figure 4.3: Test-function (left) and spherical mean values values, the equatorial cross section for $\xi_{(3)} = 0$ (middle) and a profile for $\xi = (1, 0, 0)^\top$ (right).

The spherical means $\mathcal{R}f(\xi, t)$ are the input of Algorithm 2, they are given on a standard spherical grid $\xi_{i_1,i_2} = (\sin\psi_{i_1} \cos\varphi_{i_2}, \sin\psi_{i_1} \cos\varphi_{i_2}, \cos\psi_{i_1})^\top$, where

$$\psi_{i_1} = \frac{\pi i_1}{I_1} \qquad i_1 = 0, \dots, I_1 - 1,$$
$$\varphi_{i_2} = \frac{2\pi i_2}{I_2} \qquad i_2 = 0, \dots, I_2 - 1,$$

$I = I_1 I_2$, and the discretization parameters are $I_1 = 100$, $I_2 = 200$, $M = 1500$. The remaining input parameters of Algorithm 2 are set as follows. We choose regularization parameters $q = 4$ and $\varepsilon = 4 \cdot 10^{-2}$, a cut-off degree $N = 100$, and reconstruct the test-function on a standard spherical grid $x_{j,i_1,i_2} = r_j \xi_{i_1,i_2}$ with $J = 200$ radii. The result after interpolating to a Cartesian grid and a profile for $x_{(2)} = x_{(3)} = 0$ are shown in Figure 4.4(left & middle).

As for the two-dimensional case, we consider the function $f : \mathbb{R}^3 \to \mathbb{R}$,

$$f(x) = \left(1 - \frac{|x - a|^2}{0.6^2}\right)_+^3, \quad a = \frac{1}{5}(1, 1, 1)^\top,$$

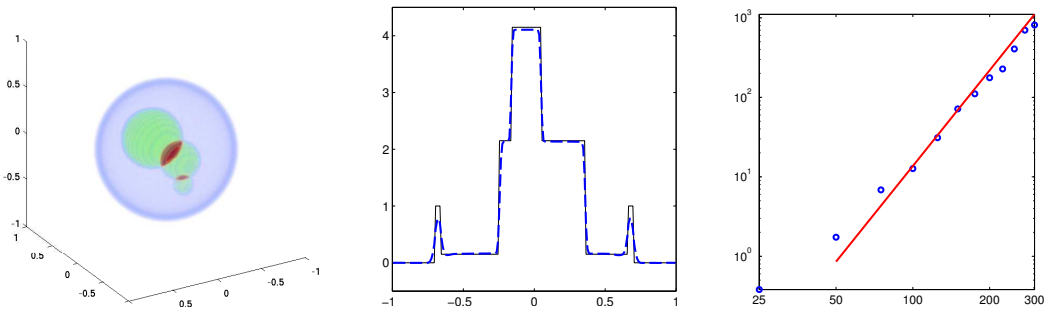

Figure 4.4: Reconstruction on a Cartesian grid (left) and a profile (dashed together with the original function) for $x_{(2)} = x_{(3)} = 0$ (middle). Computation times in seconds ($\circ$) and estimated order $\mathcal{O}\left(N^4\right)$ with respect to the common discretization parameter N (right).

for the discussion of the accuracy and computation time. Figure 4.4(right) shows the estimated arithmetic complexity $\mathcal{O}\left(N^4\right)$ and the actual time usage of Algorithm 2 for fixed regularization parameters $q = 4$, $\varepsilon = 10^{-2}$, and increasing discretization parameters $N = M = J = I_1 = I_2 = 25, 50, 75, \ldots, 300$.

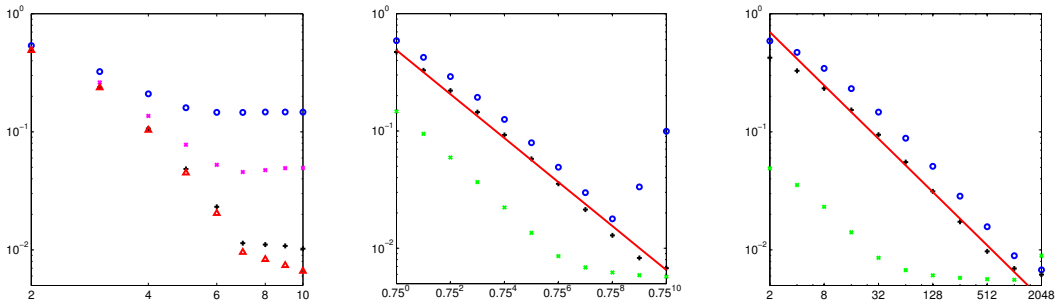

Figure 4.5: Reconstruction error E_∞ with respect to the cut-off degree N (left) and the regularization parameters ε (middle) and q (right). In the left diagram, we fixed $q = 32$ and $\varepsilon = 1, 0.5, 0.75^6, 0.1$ ($\circ$, $\times$, $+$, $\triangle$). The second diagram shows E_∞ for fixed $N = 50$ and $q = 2, 4, 32$ ($\circ$, $+$, $\times$) together with the rate $\varepsilon^{3/2}$ (solid line). In the right diagram, we consider the error with respect to q and set $N = 50$ and $\varepsilon = 1, 0.75, 0.75^6$ ($\circ$, $+$, $\times$), in addition, the rate $q^{-3/4}$ is shown (solid line).

Moreover, we consider the total accuracy (4.1) of Algorithm 2 with respect to the cut-off degree N and the regularization parameters ε, q. We fix the discretization parameters $I_1 = 100$, $I_2 = 200$, $J = 100$, and $M = 2000$. Figure 4.5(left) shows the reconstruction error for fixed regularization parameters $q = 32$, $\varepsilon = 1, 0.5, 0.75^6, 0.1$, and increasing cut-off degree $N = 2, \ldots, 10$. Surprisingly, already a small cut-off degree $N = 10$ achieves an accuracy smaller than 10^{-2} for $\varepsilon = 0.75^6, 0.1$ and we thus fix the cut-off degree $N = 50$ subsequently. Figure 4.5(middle) shows the reconstruction error for decreasing regularization parameter $\varepsilon = 0.75^l$, $l = 0, \ldots, 10$ and fixed $q = 2, 4, 32$. Up to the finally achieved accuracy, depending mainly on the time discretization M, the error decays at a rate $\varepsilon^{3/2}$. Finally, we consider E_∞ with respect to the regularization parameter $q = 2^l$, $l = 1, \ldots, 11$, and for fixed $N = 50$ and

$\varepsilon = 1, 0.75, 0.75^6$ in Figure 4.5(right). Here, the numerical error decays at a rate $q^{-3/4}$.

5 Summary

We suggested effective discretizations for the recovery of a function from its spherical means in spherical acquisition geometry. For a total problem size n, the resulting algorithms have complexity $\mathcal{O}(n^{\frac{3}{2}} \log n)$ and $\mathcal{O}(n^{\frac{4}{3}})$ for the two- and three-dimensional case, respectively. While this is still slower than the efficient schemes [10] for *exact* reconstruction formulas, it improves over the best known results [7] for *approximate* inversion.

Acknowledgment. The authors acknowledge support by the DFG within the project KU 2557/1-1 and by the Helmholtz Association within the young investigator group VH-NG-526.

References

[1] M. Ansorg, F. Filbir, W. R. Madych, and R. Seyfried. Summability kernels for circular and spherical mean data. *Inverse Problems*, 29(1):015002, 2013.

[2] V. A. Antonov, K. V. Kholshevnikov, and V. S. Shaidulin. Estimating the derivative of the Legendre polynomial. *Vestnik St. Petersburg Univ. Math.*, 43(4):191–197, 2010.

[3] F. Filbir, R. Hielscher, and W. R. Madych. Reconstruction from circular and spherical mean data. *Appl. Comput. Harmon. Anal.*, 29(1):111–120, 2010.

[4] T. Görner and S. Kunis. SMV, Matlab toolbox for computing spherical mean values. `http://www.analysis.uos.de/software`, 2012.

[5] M. Gräf, S. Kunis, and D. Potts. On the computation of nonnegative quadrature weights on the sphere. *Appl. Comput. Harmon. Anal.*, 27:124 – 132, 2009.

[6] M. Haltmeier. A mollification approach for inverting the spherical mean Radon transform. *SIAM J. Appl. Math.*, 71(5):1637–1652, 2011.

[7] M. Haltmeier, T. Schuster, and O. Scherzer. Filtered backprojection for thermoacoustic computed tomography in spherical geometry. *Math. Methods Appl. Sci.*, 28(16):1919–1937, 2005.

[8] J. Keiner, S. Kunis, and D. Potts. Fast summation of radial functions on the sphere. *Computing*, 78(1):1 – 15, 2006.

[9] J. Keiner, S. Kunis, and D. Potts. Using NFFT 3—a software library for various nonequispaced fast Fourier transforms. *ACM Trans. Math. Software*, 36(4):Art. 19, 30, 2009.

[10] L. Kunyansky. Fast reconstruction algorithms for the thermoacoustic tomography in certain domains with cylindrical or spherical symmetries. *Inverse Probl. Imaging*, 6(1):111–131, 2012.

[11] G. Szegő. *Orthogonal polynomials*. American Mathematical Society, Providence, R.I., fourth edition, 1975.

[12] L. N. Trefethen and J. A. C. Weideman. The exponentially convergent trapezoidal rule. *SIAM Rev.*, to appear.

Preprint Series DFG-SPP 1324

http://www.dfg-spp1324.de

Reports

[1] R. Ramlau, G. Teschke, and M. Zhariy. A Compressive Landweber Iteration for Solving Ill-Posed Inverse Problems. Preprint 1, DFG-SPP 1324, September 2008.

[2] G. Plonka. The Easy Path Wavelet Transform: A New Adaptive Wavelet Transform for Sparse Representation of Two-dimensional Data. Preprint 2, DFG-SPP 1324, September 2008.

[3] E. Novak and H. Woźniakowski. Optimal Order of Convergence and (In-) Tractability of Multivariate Approximation of Smooth Functions. Preprint 3, DFG-SPP 1324, October 2008.

[4] M. Espig, L. Grasedyck, and W. Hackbusch. Black Box Low Tensor Rank Approximation Using Fibre-Crosses. Preprint 4, DFG-SPP 1324, October 2008.

[5] T. Bonesky, S. Dahlke, P. Maass, and T. Raasch. Adaptive Wavelet Methods and Sparsity Reconstruction for Inverse Heat Conduction Problems. Preprint 5, DFG-SPP 1324, January 2009.

[6] E. Novak and H. Woźniakowski. Approximation of Infinitely Differentiable Multivariate Functions Is Intractable. Preprint 6, DFG-SPP 1324, January 2009.

[7] J. Ma and G. Plonka. A Review of Curvelets and Recent Applications. Preprint 7, DFG-SPP 1324, February 2009.

[8] L. Denis, D. A. Lorenz, and D. Trede. Greedy Solution of Ill-Posed Problems: Error Bounds and Exact Inversion. Preprint 8, DFG-SPP 1324, April 2009.

[9] U. Friedrich. A Two Parameter Generalization of Lions' Nonoverlapping Domain Decomposition Method for Linear Elliptic PDEs. Preprint 9, DFG-SPP 1324, April 2009.

[10] K. Bredies and D. A. Lorenz. Minimization of Non-smooth, Non-convex Functionals by Iterative Thresholding. Preprint 10, DFG-SPP 1324, April 2009.

[11] K. Bredies and D. A. Lorenz. Regularization with Non-convex Separable Constraints. Preprint 11, DFG-SPP 1324, April 2009.

[12] M. Döhler, S. Kunis, and D. Potts. Nonequispaced Hyperbolic Cross Fast Fourier Transform. Preprint 12, DFG-SPP 1324, April 2009.

[13] C. Bender. Dual Pricing of Multi-Exercise Options under Volume Constraints. Preprint 13, DFG-SPP 1324, April 2009.

[14] T. Müller-Gronbach and K. Ritter. Variable Subspace Sampling and Multi-level Algorithms. Preprint 14, DFG-SPP 1324, May 2009.

[15] G. Plonka, S. Tenorth, and A. Iske. Optimally Sparse Image Representation by the Easy Path Wavelet Transform. Preprint 15, DFG-SPP 1324, May 2009.

[16] S. Dahlke, E. Novak, and W. Sickel. Optimal Approximation of Elliptic Problems by Linear and Nonlinear Mappings IV: Errors in L_2 and Other Norms. Preprint 16, DFG-SPP 1324, June 2009.

[17] B. Jin, T. Khan, P. Maass, and M. Pidcock. Function Spaces and Optimal Currents in Impedance Tomography. Preprint 17, DFG-SPP 1324, June 2009.

[18] G. Plonka and J. Ma. Curvelet-Wavelet Regularized Split Bregman Iteration for Compressed Sensing. Preprint 18, DFG-SPP 1324, June 2009.

[19] G. Teschke and C. Borries. Accelerated Projected Steepest Descent Method for Nonlinear Inverse Problems with Sparsity Constraints. Preprint 19, DFG-SPP 1324, July 2009.

[20] L. Grasedyck. Hierarchical Singular Value Decomposition of Tensors. Preprint 20, DFG-SPP 1324, July 2009.

[21] D. Rudolf. Error Bounds for Computing the Expectation by Markov Chain Monte Carlo. Preprint 21, DFG-SPP 1324, July 2009.

[22] M. Hansen and W. Sickel. Best m-term Approximation and Lizorkin-Triebel Spaces. Preprint 22, DFG-SPP 1324, August 2009.

[23] F.J. Hickernell, T. Müller-Gronbach, B. Niu, and K. Ritter. Multi-level Monte Carlo Algorithms for Infinite-dimensional Integration on $\mathbb{R}^{\mathbb{N}}$. Preprint 23, DFG-SPP 1324, August 2009.

[24] S. Dereich and F. Heidenreich. A Multilevel Monte Carlo Algorithm for Lévy Driven Stochastic Differential Equations. Preprint 24, DFG-SPP 1324, August 2009.

[25] S. Dahlke, M. Fornasier, and T. Raasch. Multilevel Preconditioning for Adaptive Sparse Optimization. Preprint 25, DFG-SPP 1324, August 2009.

[26] S. Dereich. Multilevel Monte Carlo Algorithms for Lévy-driven SDEs with Gaussian Correction. Preprint 26, DFG-SPP 1324, August 2009.

[27] G. Plonka, S. Tenorth, and D. Roşca. A New Hybrid Method for Image Approximation using the Easy Path Wavelet Transform. Preprint 27, DFG-SPP 1324, October 2009.

[28] O. Koch and C. Lubich. Dynamical Low-rank Approximation of Tensors. Preprint 28, DFG-SPP 1324, November 2009.

[29] E. Faou, V. Gradinaru, and C. Lubich. Computing Semi-classical Quantum Dynamics with Hagedorn Wavepackets. Preprint 29, DFG-SPP 1324, November 2009.

[30] D. Conte and C. Lubich. An Error Analysis of the Multi-configuration Time-dependent Hartree Method of Quantum Dynamics. Preprint 30, DFG-SPP 1324, November 2009.

[31] C. E. Powell and E. Ullmann. Preconditioning Stochastic Galerkin Saddle Point Problems. Preprint 31, DFG-SPP 1324, November 2009.

[32] O. G. Ernst and E. Ullmann. Stochastic Galerkin Matrices. Preprint 32, DFG-SPP 1324, November 2009.

[33] F. Lindner and R. L. Schilling. Weak Order for the Discretization of the Stochastic Heat Equation Driven by Impulsive Noise. Preprint 33, DFG-SPP 1324, November 2009.

[34] L. Kämmerer and S. Kunis. On the Stability of the Hyperbolic Cross Discrete Fourier Transform. Preprint 34, DFG-SPP 1324, December 2009.

[35] P. Cerejeiras, M. Ferreira, U. Kähler, and G. Teschke. Inversion of the noisy Radon transform on $SO(3)$ by Gabor frames and sparse recovery principles. Preprint 35, DFG-SPP 1324, January 2010.

[36] T. Jahnke and T. Udrescu. Solving Chemical Master Equations by Adaptive Wavelet Compression. Preprint 36, DFG-SPP 1324, January 2010.

[37] P. Kittipoom, G. Kutyniok, and W.-Q Lim. Irregular Shearlet Frames: Geometry and Approximation Properties. Preprint 37, DFG-SPP 1324, February 2010.

[38] G. Kutyniok and W.-Q Lim. Compactly Supported Shearlets are Optimally Sparse. Preprint 38, DFG-SPP 1324, February 2010.

[39] M. Hansen and W. Sickel. Best m-Term Approximation and Tensor Products of Sobolev and Besov Spaces – the Case of Non-compact Embeddings. Preprint 39, DFG-SPP 1324, March 2010.

[40] B. Niu, F.J. Hickernell, T. Müller-Gronbach, and K. Ritter. Deterministic Multi-level Algorithms for Infinite-dimensional Integration on $\mathbb{R}^{\mathbb{N}}$. Preprint 40, DFG-SPP 1324, March 2010.

[41] P. Kittipoom, G. Kutyniok, and W.-Q Lim. Construction of Compactly Supported Shearlet Frames. Preprint 41, DFG-SPP 1324, March 2010.

[42] C. Bender and J. Steiner. Error Criteria for Numerical Solutions of Backward SDEs. Preprint 42, DFG-SPP 1324, April 2010.

[43] L. Grasedyck. Polynomial Approximation in Hierarchical Tucker Format by Vector-Tensorization. Preprint 43, DFG-SPP 1324, April 2010.

[44] M. Hansen und W. Sickel. Best m-Term Approximation and Sobolev-Besov Spaces of Dominating Mixed Smoothness - the Case of Compact Embeddings. Preprint 44, DFG-SPP 1324, April 2010.

[45] P. Binev, W. Dahmen, and P. Lamby. Fast High-Dimensional Approximation with Sparse Occupancy Trees. Preprint 45, DFG-SPP 1324, May 2010.

[46] J. Ballani and L. Grasedyck. A Projection Method to Solve Linear Systems in Tensor Format. Preprint 46, DFG-SPP 1324, May 2010.

[47] P. Binev, A. Cohen, W. Dahmen, R. DeVore, G. Petrova, and P. Wojtaszczyk. Convergence Rates for Greedy Algorithms in Reduced Basis Methods. Preprint 47, DFG-SPP 1324, May 2010.

[48] S. Kestler and K. Urban. Adaptive Wavelet Methods on Unbounded Domains. Preprint 48, DFG-SPP 1324, June 2010.

[49] H. Yserentant. The Mixed Regularity of Electronic Wave Functions Multiplied by Explicit Correlation Factors. Preprint 49, DFG-SPP 1324, June 2010.

[50] H. Yserentant. On the Complexity of the Electronic Schrödinger Equation. Preprint 50, DFG-SPP 1324, June 2010.

[51] M. Guillemard and A. Iske. Curvature Analysis of Frequency Modulated Manifolds in Dimensionality Reduction. Preprint 51, DFG-SPP 1324, June 2010.

[52] E. Herrholz and G. Teschke. Compressive Sensing Principles and Iterative Sparse Recovery for Inverse and Ill-Posed Problems. Preprint 52, DFG-SPP 1324, July 2010.

[53] L. Kämmerer, S. Kunis, and D. Potts. Interpolation Lattices for Hyperbolic Cross Trigonometric Polynomials. Preprint 53, DFG-SPP 1324, July 2010.

[54] G. Kutyniok and W.-Q Lim. Shearlets on Bounded Domains. Preprint 54, DFG-SPP 1324, July 2010.

[55] A. Zeiser. Wavelet Approximation in Weighted Sobolev Spaces of Mixed Order with Applications to the Electronic Schrödinger Equation. Preprint 55, DFG-SPP 1324, July 2010.

[56] G. Kutyniok, J. Lemvig, and W.-Q Lim. Compactly Supported Shearlets. Preprint 56, DFG-SPP 1324, July 2010.

[57] A. Zeiser. On the Optimality of the Inexact Inverse Iteration Coupled with Adaptive Finite Element Methods. Preprint 57, DFG-SPP 1324, July 2010.

[58] S. Jokar. Sparse Recovery and Kronecker Products. Preprint 58, DFG-SPP 1324, August 2010.

[59] T. Aboiyar, E. H. Georgoulis, and A. Iske. Adaptive ADER Methods Using Kernel-Based Polyharmonic Spline WENO Reconstruction. Preprint 59, DFG-SPP 1324, August 2010.

[60] O. G. Ernst, A. Mugler, H.-J. Starkloff, and E. Ullmann. On the Convergence of Generalized Polynomial Chaos Expansions. Preprint 60, DFG-SPP 1324, August 2010.

[61] S. Holtz, T. Rohwedder, and R. Schneider. On Manifolds of Tensors of Fixed TT-Rank. Preprint 61, DFG-SPP 1324, September 2010.

[62] J. Ballani, L. Grasedyck, and M. Kluge. Black Box Approximation of Tensors in Hierarchical Tucker Format. Preprint 62, DFG-SPP 1324, October 2010.

[63] M. Hansen. On Tensor Products of Quasi-Banach Spaces. Preprint 63, DFG-SPP 1324, October 2010.

[64] S. Dahlke, G. Steidl, and G. Teschke. Shearlet Coorbit Spaces: Compactly Supported Analyzing Shearlets, Traces and Embeddings. Preprint 64, DFG-SPP 1324, October 2010.

[65] W. Hackbusch. Tensorisation of Vectors and their Efficient Convolution. Preprint 65, DFG-SPP 1324, November 2010.

[66] P. A. Cioica, S. Dahlke, S. Kinzel, F. Lindner, T. Raasch, K. Ritter, and R. L. Schilling. Spatial Besov Regularity for Stochastic Partial Differential Equations on Lipschitz Domains. Preprint 66, DFG-SPP 1324, November 2010.

[67] E. Novak and H. Woźniakowski. On the Power of Function Values for the Approximation Problem in Various Settings. Preprint 67, DFG-SPP 1324, November 2010.

[68] A. Hinrichs, E. Novak, and H. Woźniakowski. The Curse of Dimensionality for Monotone and Convex Functions of Many Variables. Preprint 68, DFG-SPP 1324, November 2010.

[69] G. Kutyniok and W.-Q Lim. Image Separation Using Shearlets. Preprint 69, DFG-SPP 1324, November 2010.

[70] B. Jin and P. Maass. An Analysis of Electrical Impedance Tomography with Applications to Tikhonov Regularization. Preprint 70, DFG-SPP 1324, December 2010.

[71] S. Holtz, T. Rohwedder, and R. Schneider. The Alternating Linear Scheme for Tensor Optimisation in the TT Format. Preprint 71, DFG-SPP 1324, December 2010.

[72] T. Müller-Gronbach and K. Ritter. A Local Refinement Strategy for Constructive Quantization of Scalar SDEs. Preprint 72, DFG-SPP 1324, December 2010.

[73] T. Rohwedder and R. Schneider. An Analysis for the DIIS Acceleration Method used in Quantum Chemistry Calculations. Preprint 73, DFG-SPP 1324, December 2010.

[74] C. Bender and J. Steiner. Least-Squares Monte Carlo for Backward SDEs. Preprint 74, DFG-SPP 1324, December 2010.

[75] C. Bender. Primal and Dual Pricing of Multiple Exercise Options in Continuous Time. Preprint 75, DFG-SPP 1324, December 2010.

[76] H. Harbrecht, M. Peters, and R. Schneider. On the Low-rank Approximation by the Pivoted Cholesky Decomposition. Preprint 76, DFG-SPP 1324, December 2010.

[77] P. A. Cioica, S. Dahlke, N. Döhring, S. Kinzel, F. Lindner, T. Raasch, K. Ritter, and R. L. Schilling. Adaptive Wavelet Methods for Elliptic Stochastic Partial Differential Equations. Preprint 77, DFG-SPP 1324, January 2011.

[78] G. Plonka, S. Tenorth, and A. Iske. Optimal Representation of Piecewise Hölder Smooth Bivariate Functions by the Easy Path Wavelet Transform. Preprint 78, DFG-SPP 1324, January 2011.

[79] A. Mugler and H.-J. Starkloff. On Elliptic Partial Differential Equations with Random Coefficients. Preprint 79, DFG-SPP 1324, January 2011.

[80] T. Müller-Gronbach, K. Ritter, and L. Yaroslavtseva. A Derandomization of the Euler Scheme for Scalar Stochastic Differential Equations. Preprint 80, DFG-SPP 1324, January 2011.

[81] W. Dahmen, C. Huang, C. Schwab, and G. Welper. Adaptive Petrov-Galerkin methods for first order transport equations. Preprint 81, DFG-SPP 1324, January 2011.

[82] K. Grella and C. Schwab. Sparse Tensor Spherical Harmonics Approximation in Radiative Transfer. Preprint 82, DFG-SPP 1324, January 2011.

[83] D.A. Lorenz, S. Schiffler, and D. Trede. Beyond Convergence Rates: Exact Inversion With Tikhonov Regularization With Sparsity Constraints. Preprint 83, DFG-SPP 1324, January 2011.

[84] S. Dereich, M. Scheutzow, and R. Schottstedt. Constructive quantization: Approximation by empirical measures. Preprint 84, DFG-SPP 1324, January 2011.

[85] S. Dahlke and W. Sickel. On Besov Regularity of Solutions to Nonlinear Elliptic Partial Differential Equations. Preprint 85, DFG-SPP 1324, January 2011.

[86] S. Dahlke, U. Friedrich, P. Maass, T. Raasch, and R.A. Ressel. An adaptive wavelet method for parameter identification problems in parabolic partial differential equations. Preprint 86, DFG-SPP 1324, January 2011.

[87] A. Cohen, W. Dahmen, and G. Welper. Adaptivity and Variational Stabilization for Convection-Diffusion Equations. Preprint 87, DFG-SPP 1324, January 2011.

[88] T. Jahnke. On Reduced Models for the Chemical Master Equation. Preprint 88, DFG-SPP 1324, January 2011.

[89] P. Binev, W. Dahmen, R. DeVore, P. Lamby, D. Savu, and R. Sharpley. Compressed Sensing and Electron Microscopy. Preprint 89, DFG-SPP 1324, March 2011.

[90] P. Binev, F. Blanco-Silva, D. Blom, W. Dahmen, P. Lamby, R. Sharpley, and T. Vogt. High Quality Image Formation by Nonlocal Means Applied to High-Angle Annular Dark Field Scanning Transmission Electron Microscopy (HAADF-STEM). Preprint 90, DFG-SPP 1324, March 2011.

[91] R. A. Ressel. A Parameter Identification Problem for a Nonlinear Parabolic Differential Equation. Preprint 91, DFG-SPP 1324, May 2011.

[92] G. Kutyniok. Data Separation by Sparse Representations. Preprint 92, DFG-SPP 1324, May 2011.

[93] M. A. Davenport, M. F. Duarte, Y. C. Eldar, and G. Kutyniok. Introduction to Compressed Sensing. Preprint 93, DFG-SPP 1324, May 2011.

[94] H.-C. Kreusler and H. Yserentant. The Mixed Regularity of Electronic Wave Functions in Fractional Order and Weighted Sobolev Spaces. Preprint 94, DFG-SPP 1324, June 2011.

[95] E. Ullmann, H. C. Elman, and O. G. Ernst. Efficient Iterative Solvers for Stochastic Galerkin Discretizations of Log-Transformed Random Diffusion Problems. Preprint 95, DFG-SPP 1324, June 2011.

[96] S. Kunis and I. Melzer. On the Butterfly Sparse Fourier Transform. Preprint 96, DFG-SPP 1324, June 2011.

[97] T. Rohwedder. The Continuous Coupled Cluster Formulation for the Electronic Schrödinger Equation. Preprint 97, DFG-SPP 1324, June 2011.

[98] T. Rohwedder and R. Schneider. Error Estimates for the Coupled Cluster Method. Preprint 98, DFG-SPP 1324, June 2011.

[99] P. A. Cioica and S. Dahlke. Spatial Besov Regularity for Semilinear Stochastic Partial Differential Equations on Bounded Lipschitz Domains. Preprint 99, DFG-SPP 1324, July 2011.

[100] L. Grasedyck and W. Hackbusch. An Introduction to Hierarchical (H-) Rank and TT-Rank of Tensors with Examples. Preprint 100, DFG-SPP 1324, August 2011.

[101] N. Chegini, S. Dahlke, U. Friedrich, and R. Stevenson. Piecewise Tensor Product Wavelet Bases by Extensions and Approximation Rates. Preprint 101, DFG-SPP 1324, September 2011.

[102] S. Dahlke, P. Oswald, and T. Raasch. A Note on Quarkonial Systems and Multilevel Partition of Unity Methods. Preprint 102, DFG-SPP 1324, September 2011.

[103] A. Uschmajew. Local Convergence of the Alternating Least Squares Algorithm For Canonical Tensor Approximation. Preprint 103, DFG-SPP 1324, September 2011.

[104] S. Kvaal. Multiconfigurational time-dependent Hartree method for describing particle loss due to absorbing boundary conditions. Preprint 104, DFG-SPP 1324, September 2011.

[105] M. Guillemard and A. Iske. On Groupoid C*-Algebras, Persistent Homology and Time-Frequency Analysis. Preprint 105, DFG-SPP 1324, September 2011.

[106] A. Hinrichs, E. Novak, and H. Woźniakowski. Discontinuous information in the worst case and randomized settings. Preprint 106, DFG-SPP 1324, September 2011.

[107] M. Espig, W. Hackbusch, A. Litvinenko, H. Matthies, and E. Zander. Efficient Analysis of High Dimensional Data in Tensor Formats. Preprint 107, DFG-SPP 1324, September 2011.

[108] M. Espig, W. Hackbusch, S. Handschuh, and R. Schneider. Optimization Problems in Contracted Tensor Networks. Preprint 108, DFG-SPP 1324, October 2011.

[109] S. Dereich, T. Müller-Gronbach, and K. Ritter. On the Complexity of Computing Quadrature Formulas for SDEs. Preprint 109, DFG-SPP 1324, October 2011.

[110] D. Belomestny. Solving optimal stopping problems by empirical dual optimization and penalization. Preprint 110, DFG-SPP 1324, November 2011.

[111] D. Belomestny and J. Schoenmakers. Multilevel dual approach for pricing American style derivatives. Preprint 111, DFG-SPP 1324, November 2011.

[112] T. Rohwedder and A. Uschmajew. Local convergence of alternating schemes for optimization of convex problems in the TT format. Preprint 112, DFG-SPP 1324, December 2011.

[113] T. Görner, R. Hielscher, and S. Kunis. Efficient and accurate computation of spherical mean values at scattered center points. Preprint 113, DFG-SPP 1324, December 2011.

[114] Y. Dong, T. Görner, and S. Kunis. An iterative reconstruction scheme for photoacoustic imaging. Preprint 114, DFG-SPP 1324, December 2011.

[115] L. Kämmerer. Reconstructing hyperbolic cross trigonometric polynomials by sampling along generated sets. Preprint 115, DFG-SPP 1324, February 2012.

[116] H. Chen and R. Schneider. Numerical analysis of augmented plane waves methods for full-potential electronic structure calculations. Preprint 116, DFG-SPP 1324, February 2012.

[117] J. Ma, G. Plonka, and M.Y. Hussaini. Compressive Video Sampling with Approximate Message Passing Decoding. Preprint 117, DFG-SPP 1324, February 2012.

[118] D. Heinen and G. Plonka. Wavelet shrinkage on paths for scattered data denoising. Preprint 118, DFG-SPP 1324, February 2012.

[119] T. Jahnke and M. Kreim. Error bound for piecewise deterministic processes modeling stochastic reaction systems. Preprint 119, DFG-SPP 1324, March 2012.

[120] C. Bender and J. Steiner. A-posteriori estimates for backward SDEs. Preprint 120, DFG-SPP 1324, April 2012.

[121] M. Espig, W. Hackbusch, A. Litvinenkoy, H.G. Matthiesy, and P. Wähnert. Effcient low-rank approximation of the stochastic Galerkin matrix in tensor formats. Preprint 121, DFG-SPP 1324, May 2012.

[122] O. Bokanowski, J. Garcke, M. Griebel, and I. Klompmaker. An adaptive sparse grid semi-Lagrangian scheme for first order Hamilton-Jacobi Bellman equations. Preprint 122, DFG-SPP 1324, June 2012.

[123] A. Mugler and H.-J. Starkloff. On the convergence of the stochastic Galerkin method for random elliptic partial differential equations. Preprint 123, DFG-SPP 1324, June 2012.

[124] P.A. Cioica, S. Dahlke, N. Döhring, U. Friedrich, S. Kinzel, F. Lindner, T. Raasch, K. Ritter, and R.L. Schilling. On the convergence analysis of Rothe's method. Preprint 124, DFG-SPP 1324, July 2012.

[125] P. Binev, A. Cohen, W. Dahmen, and R. DeVore. Classification Algorithms using Adaptive Partitioning. Preprint 125, DFG-SPP 1324, July 2012.

[126] C. Lubich, T. Rohwedder, R. Schneider, and B. Vandereycken. Dynamical approximation of hierarchical Tucker and Tensor-Train tensors. Preprint 126, DFG-SPP 1324, July 2012.

[127] M. Kovács, S. Larsson, and K. Urban. On Wavelet-Galerkin methods for semilinear parabolic equations with additive noise. Preprint 127, DFG-SPP 1324, August 2012.

[128] M. Bachmayr, H. Chen, and R. Schneider. Numerical analysis of Gaussian approximations in quantum chemistry. Preprint 128, DFG-SPP 1324, August 2012.

[129] D. Rudolf. Explicit error bounds for Markov chain Monte Carlo. Preprint 129, DFG-SPP 1324, August 2012.

[130] P.A. Cioica, K.-H. Kim, K. Lee, and F. Lindner. On the $L_q(L_p)$-regularity and Besov smoothness of stochastic parabolic equations on bounded Lipschitz domains. Preprint 130, DFG-SPP 1324, December 2012.

[131] M. Hansen. $n-$term Approximation Rates and Besov Regularity for Elliptic PDEs on Polyhedral Domains. Preprint 131, DFG-SPP 1324, December 2012.

[132] R. E. Bank and H. Yserentant. On the H^1 -stability of the L_2 -projection onto finite element spaces. Preprint 132, DFG-SPP 1324, December 2012.

[133] M. Gnewuch, S. Mayer, and K. Ritter. On Weighted Hilbert Spaces and Integration of Functions of Infinitely Many Variables. Preprint 133, DFG-SPP 1324, December 2012.

[134] D. Crisan, J. Diehl, P.K. Friz, and H. Oberhauser. Robust Filtering: Correlated Noise and Multidimensional Observation. Preprint 134, DFG-SPP 1324, January 2013.

[135] Wolfgang Dahmen, Christian Plesken, and Gerrit Welper. Double Greedy Algorithms: Reduced Basis Methods for Transport Dominated Problems. Preprint 135, DFG-SPP 1324, February 2013.

[136] Aicke Hinrichs, Erich Novak, Mario Ullrich, and Henryk Wozniakowski. The Curse of Dimensionality for Numerical Integration of Smooth Functions. Preprint 136, DFG-SPP 1324, February 2013.

[137] Markus Bachmayr, Wolfgang Dahmen, Ronald DeVore, and Lars Grasedyck. Approximation of High-Dimensional Rank One Tensors. Preprint 137, DFG-SPP 1324, March 2013.

[138] Markus Bachmayr and Wolfgang Dahmen. Adaptive Near-Optimal Rank Tensor Approximation for High-Dimensional Operator Equations. Preprint 138, DFG-SPP 1324, April 2013.

[139] Felix Lindner. Singular Behavior of the Solution to the Stochastic Heat Equation on a Polygonal Domain. Preprint 139, DFG-SPP 1324, May 2013.

[140] Stephan Dahlke, Dominik Lellek, Shiu Hong Lui, and Rob Stevenson. Adaptive Wavelet Schwarz Methods for the Navier-Stokes Equation. Preprint 140, DFG-SPP 1324, May 2013.

[141] Jonas Ballani and Lars Grasedyck. Tree Adaptive Approximation in the Hierarchical Tensor Format. Preprint 141, DFG-SPP 1324, June 2013.

[142] Harry Yserentant. A short theory of the Rayleigh-Ritz method. Preprint 142, DFG-SPP 1324, July 2013.

[143] M. Hefter and K. Ritter. On Embeddings of Weighted Tensor Product Hilbert Spaces. Preprint 143, DFG-SPP 1324, August 2013.

[144] M. Altmayer and A. Neuenkirch. Multilevel Monte Carlo Quadrature of Discontinuous Payoffs in the Generalized Heston Model using Malliavin Integration by Parts. Preprint 144, DFG-SPP 1324, August 2013.

[145] L. Kämmerer, D. Potts, and T. Volkmer. Approximation of multivariate functions by trigonometric polynomials based on rank-1 lattice sampling. Preprint 145, DFG-SPP 1324, September 2013.

[146] C. Bender, N. Schweizer, and J. Zhuo. A primal-dual algorithm for BSDEs. Preprint 146, DFG-SPP 1324, October 2013.

[147] D. Rudolf. Hit-and-run for numerical integration. Preprint 147, DFG-SPP 1324, October 2013.

[148] D. Rudolf and M. Ullrich. Positivity of hit-and-run and related algorithms. Preprint 148, DFG-SPP 1324, October 2013.

[149] L. Grasedyck, M. Kluge, and S. Krämer. Alternating Directions Fitting (ADF) of Hierarchical Low Rank Tensors. Preprint 149, DFG-SPP 1324, October 2013.

[150] F. Filbir, S. Kunis, and R. Seyfried. Effective discretization of direct reconstruction schemes for photoacoustic imaging in spherical geometries. Preprint 150, DFG-SPP 1324, November 2013.